Experimental Facilities

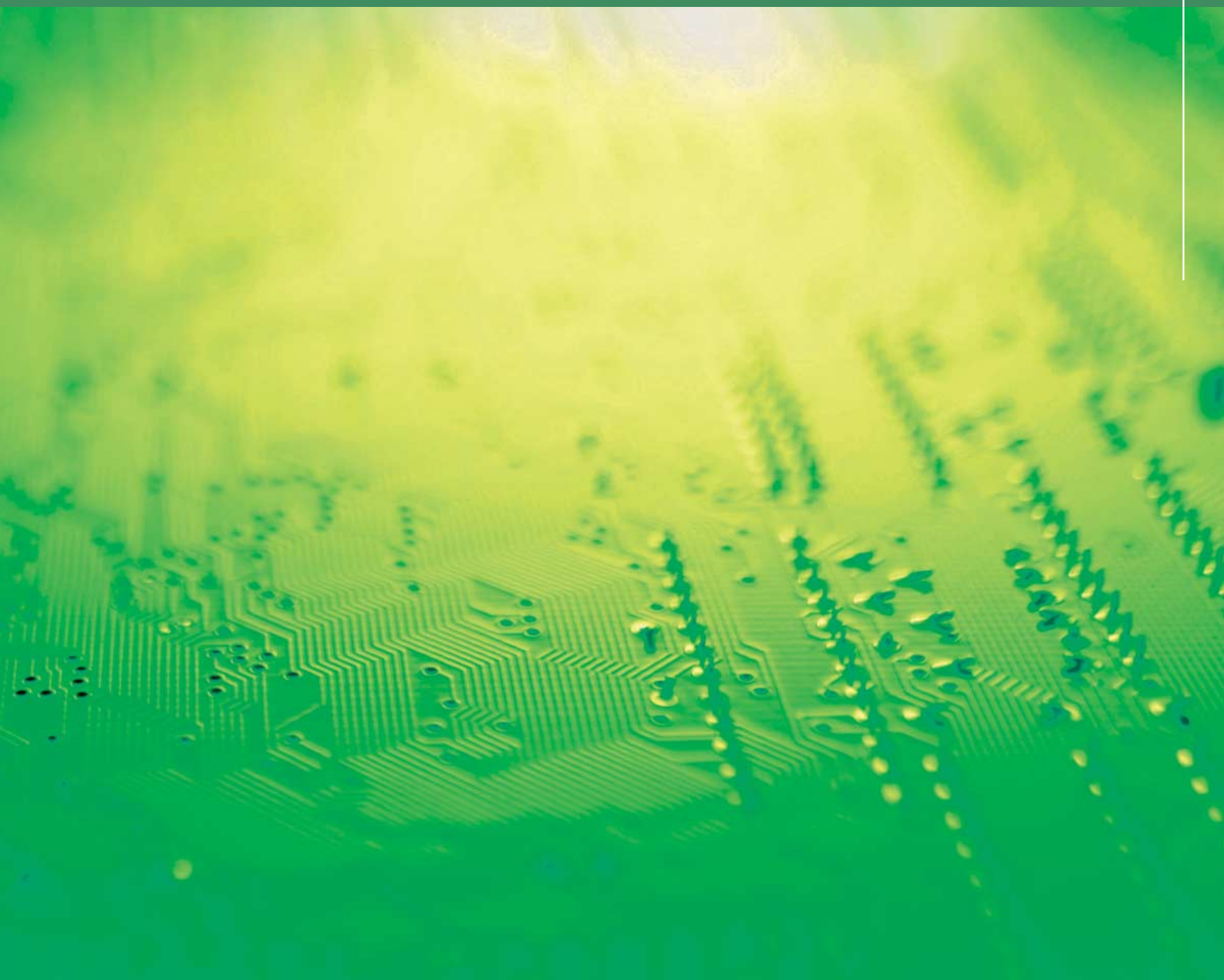

EXPERIMENTAL FACILITIES

1 Summary of Experimental Stations

There are 70 experimental stations on the PF storage ring and the PF-AR, as shown in Figs. 1 and 2. Two thirds of them are dedicated for research using hard X-rays, while the rest one third in the VUV and soft X-ray region. These experimental stations are summarized to designate research fields carried out on them in Tables 1 and 2, respectively, for the PF storage ring and PF-AR.

Each experimental station has a different specification in optics and performance depending on the methodology performed. Tables 3 and 4 list the optics of hard X-ray and soft X-ray or VUV stations, respectively, together with the principal performances, such as energy range, spot size, photon flux and energy resolution.

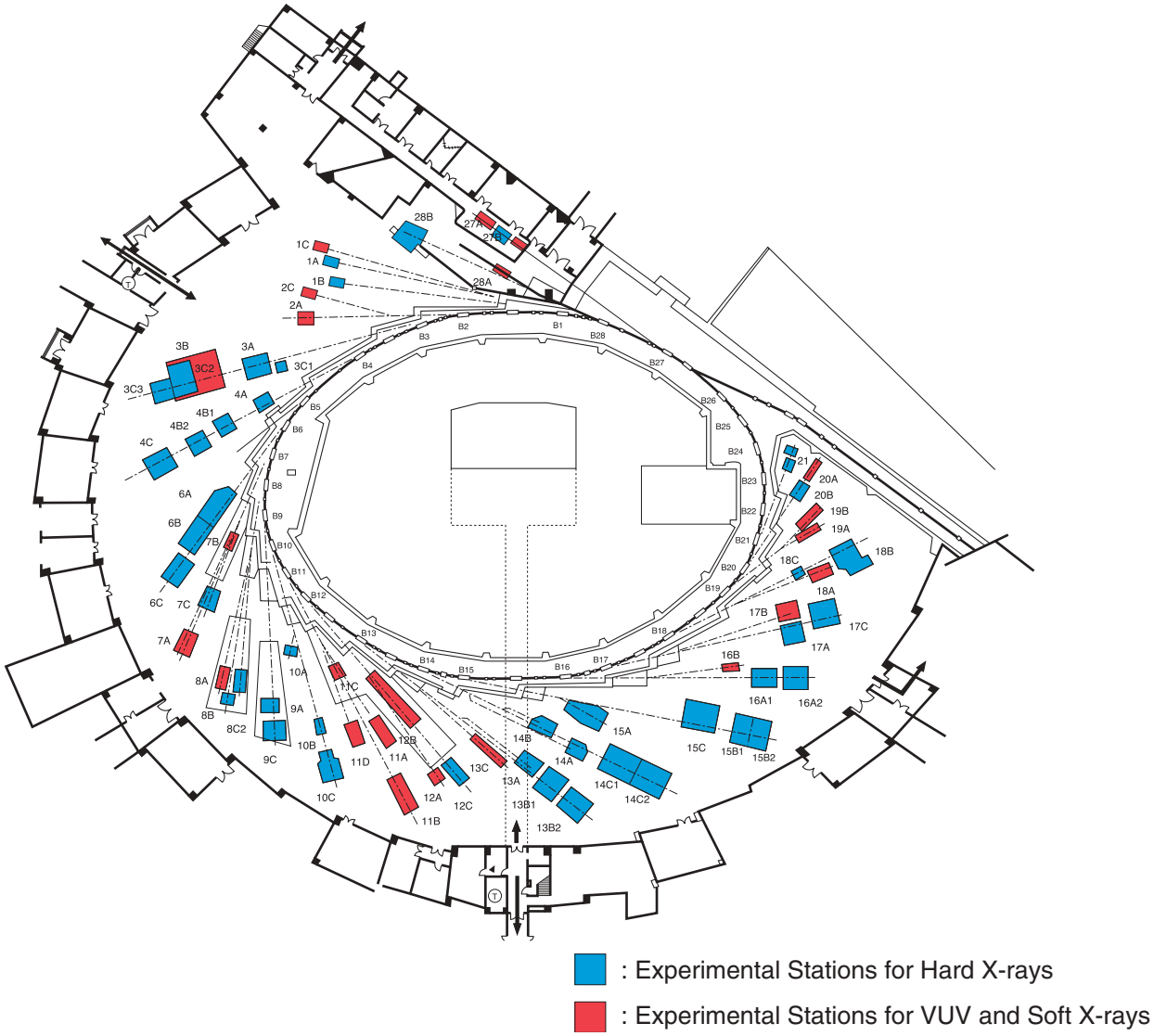

Figure 1
Plan view of the PF experimental hall.

Table 1 List of Experimental Stations at the PF Storage Ring.

Experimental Station			Spokesperson
BL-1			
	A	Crystal Structure dnalysis beamline of collaboratory (under construction)	H. Sawa
	B	X-ray powder diffraction under extreme condition	H. Sawa
	C	VUV and soft X-ray photoelectron spectroscopy	M. Nakatake
BL-2		(Undulator)	
	A	Soft X-ray spectroscopy	Y. Kitajima
	C	Soft X-ray spectroscopy	A. Yagishita
BL-3			
	A	X-ray diffraction and scattering	M. Tanaka
	B	VUV and soft X-ray spectroscopy	Y. Azuma
	C1	X-ray diffraction	H. Adachi, H. Kawata
	C2	Characterization of X-ray optical elements	M. Ando
	C3	X-ray magnetic Bragg scattering by means of white X-rays	H. Adachi, H. Kawata
BL-4			
	A	Trace element analysis, X-ray microprobe	A. Iida
	B1	Micro-crystal and -area structure analysis	K. Ohsumi
	B2	Powder diffraction	M. Tanaka
	C	X-ray diffraction and scattering	Y. Wakabayashi
BL-6			
	A	Macromolecular crystallography	N. Igarashi
	B	[SBSP]Macromolecular crystallography by Weissenberg camera	N. Sakabe[SBSP], M. Suzuki
	C	[SBSP]Macromolecular crystallography by Weissenberg camera	N. Sakabe[SBSP], M. Suzuki
BL-7			
	A	[RCS]Soft X-ray XAFS, XMCD, XPS	K. Amemiya[RCS], K. Ito
	B	[RCS]Surface photochemical reaction and angle resolved photoelectron spectroscopy	K. Amemiya[RCS], K. Ito
	C	X-ray spectroscopy and diffraction	T. Iwazumi
BL-8			
	A	[Hitachi]Soft X-ray spectroscopy	K. Ogata[Hitachi], K. Mase
	B	[Hitachi]EXAFS	K. Ogata[Hitachi], K. Mase
	C	[Hitachi]X-ray tomography and X-ray microscopy	K. Ogata[Hitachi], K. Mase
BL-9			
	A	XAFS	M. Nomura
	C	X-ray versatile station	M. Nomura
BL-10			
	A	X-ray diffraction/scattering	M. Tanaka
	B	XAFS	N. Usami
	C	Small-angle X-ray scattering of solution sample	K. Kobayashi
BL-11			
	A	Soft X-ray spectroscopy	Y. Kitajima
	B	Surface EXAFS, soft X-ray spectroscopy	Y. Kitajima
	C	VUV spectroscopy (solid state)	M. Nakatake
	D	VUV and soft X-ray photoelectron spectroscopy for solid	M. Nakatake
BL-12			
	A	Characterization of VUV-SX optical elements, soft X-ray spectroscopy	A. Yagishita
	B	VUV high-resolution spectroscopy	K. Ito
	C	XAFS	M. Nomura

Experimental Station		Spokesperson
BL-13	(Multipole Wiggler/Undulator)	
A	Laser-heating high-pressure and high-temperature X-ray diffraction (DAC)	T. Kikegawa
B1	Surface-sensitive XAFS, X-ray diffraction	T. Kikegawa
B2	High-pressure and high-temperature X-ray diffraction	T. Kikegawa
C	Soft X-ray photoemission spectroscopy and XAFS	K. Mase
BL-14	(Vertical Wiggler)	
A	Crystal structure analysis, EXAFS	S. Kishimoto
B	High-precision X-ray optics	K. Hirano
C1	Medical applications and General purpose (X-ray)	K. Hyodo
C2	High-pressure and high-temperature X-ray diffraction (MAX-III)	T. Kikegawa
BL-15		
A	Small-angle X-ray scattering of muscle and alloys	M. Suzuki
B1	White X-ray topography and X-ray magnetic Bragg scattering	H. Sugiyama
B2	Surface and interface diffraction	H. Sugiyama, H. Kawata
C	High-resolution X-ray diffraction	K. Hirano
BL-16	(Multipole Wiggler/Undulator)	
A1	General purpose (X-ray)	Y. Wakabayashi
A2	X-ray diffraction and scattering	Y. Wakabayashi
B	Soft X-ray spectroscopy	J. Adachi
BL-17		
A	[Fujitsu]XAFS	N. Awaji[Fujitsu], A. Iida
B	[Fujitsu]Photochemical vapor deposition	N. Awaji[Fujitsu], A. Iida
C	[Fujitsu]Grazing incident X-ray diffraction, X-ray fluorescence analysis	N. Awaji[Fujitsu], A. Iida
BL-18		
A	[ISSP]Angle-resolved photoelectron spectroscopy of surfaces and interfaces	T. Kinoshita[ISSP], A. Yagishita
B	Macromolecular crystallography	M. Suzuki
C	High pressure X-ray powder diffraction (DAC)	T. Kikegawa
BL-19	(Revolver Undulator)	
A	[ISSP]Spin-resolved photoelectron spectroscopy (Mott detector)	T. Kinoshita[ISSP], A. Yagishita
B	[ISSP]Spin-resolved photoelectron spectroscopy (SPLEED) [ISSP]Soft X-ray emission spectroscopy	S. Shin[ISSP], A. Yagishita
BL-20		
A	VUV spectroscopy	K. Ito
B	[ANBF]White and monochromatic beam general purpose X-ray station	G. Foran[ANBF], K. Ohsumi
BL-21	[Light Source Division]Beam position monitoring	M. Kobayashi[Light Source]
BL-27	(Beamline for experiments using radioisotopes)	
A	Radiation biology, soft X-ray photoelectron spectroscopy	K. Kobayashi
B	Radiation biology, XAFS, X-ray diffuse scattering	N. Usami
BL-28	(Elliptical Multipole Wiggler / Helical Undulator)	
A	VUV and soft X-ray spectroscopy with circularly polarized undulator radiation	T. Koide
B	Spectroscopy and scattering with circularly polarized X-rays	T. Iwazumi

SBSP Structural Biology Sakabe Project, Foundation for Advancement of International Science
RCS Research Center for Spectrochemistry, the University of Tokyo
ISSP Institute for Solid State Physics, the University of Tokyo
ANBF Australian National Beamline Facility

Table 2 List of Experimental Stations at the PF-AR.

Experimental Station	Spokesperson
AR-NE1 (Elliptical Multipole Wiggler / Helical Undulator)	
A1 High-resolution Compton and magnetic Compton scattering	H. Kawata
A2 Coronary Angiography	K. Hyodo
B Spectroscopy with circularly polarized soft X-rays	T. Koide
AR-NE3 (Undulator)	
A Nuclear resonant scattering	X. Zhang
AR-NE5	
A Medical applications	K. Hyodo
B Bunch-purity and beam-position monitoring	S. Kishimoto
C High pressure and high temperature X-ray diffraction (MAX-80)	T. Kikegawa
AR-NE9	
B [Accelerator Laboratory]Vacuum science and technology	K. Kanazawa[Acc.Lab.]
AR-NW2 (Undulator)	
A XAFS/Dispersive XAFS (under construction)	H. Kawata
AR-NW12 (Undulator)	
A Macromolecular crystallography (under construction)	N. Matsugaki

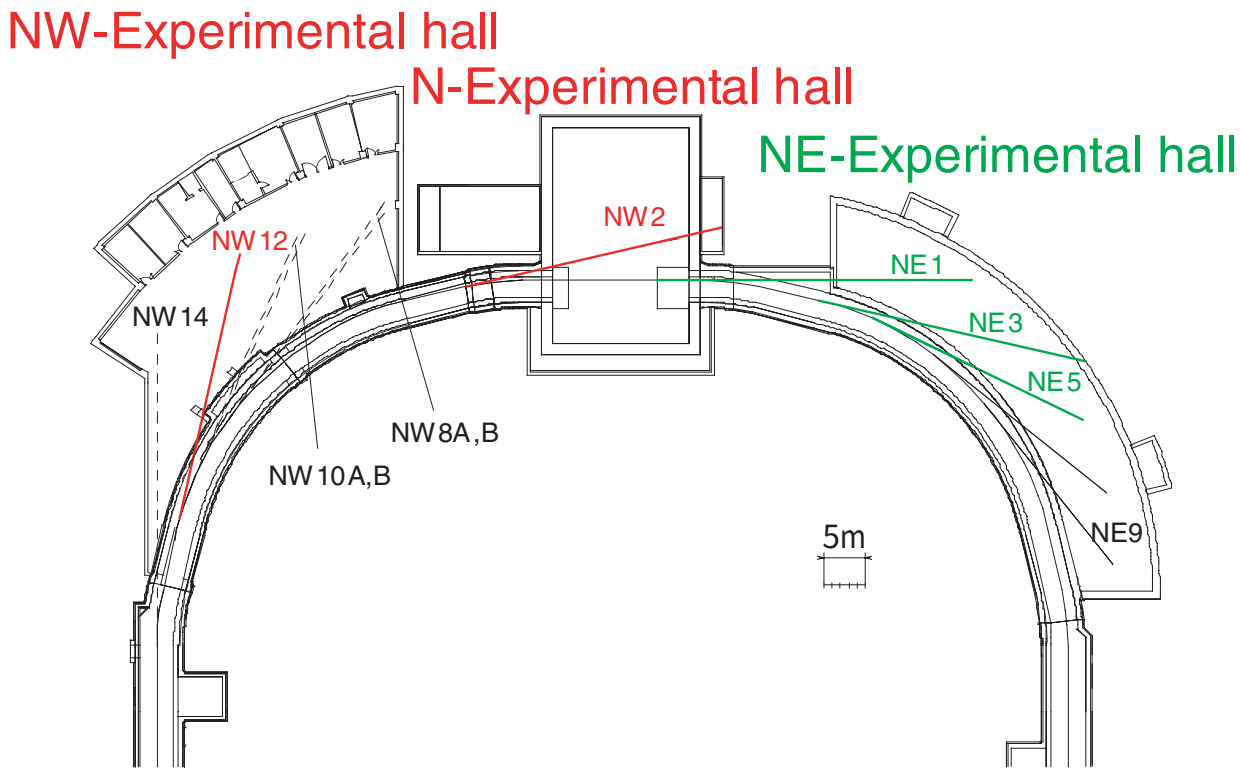

Figure 2
Plan view of the beamlines in the PF-AR north-east, north, and north-west experimental halls.

Table 3 X-Ray Beamline Optics.

Branch Beamline	Horizontal Acceptance (mrad)	Type of Monochromator	Mirror	Photon Energy (keV)	Beam Size (H×V) (mm)	Photon Flux at Sample Position (/s)	Energy Resolution ($\Delta E/E$)×10^{-4}	Reference
BL-1B	2	Flat Double Crystal Si(111)	Bent Cylinder	6 ~ 21	0.7×0.5	8×10^{10}/4mm^2 (8.3 keV, 300 mA)	~ 5	1
BL-3A	4	Double Crystal Si(111) Sagittal Focusing	Collimating Focusing Mirrors (Fused Quartz)	6 ~ 20	100×5 2×1		~ 2	2 - 4
BL-3C2	2	Double Crystal Si(111), Si(311)	None	4 ~ 20 6 ~ 34	5×2	1×10^{10} 2×10^{9}		
BL-3C3	2	Double Crystal Si(111)	None	5 ~ 30 or white	20×4 0.1×0.1			
BL-4A	6	Double Crystal Sagittal Focusing	None	4 ~ 20	50×4 4×1		~ 2	5
BL-4B1	4.5	Double Crystal Si(111)	None	4 ~ 35	50×5		~ 2	6
BL-4B2	4.5	Double Crystal Si(111)	Bent Cylinder	6 ~ 20	13×2		~2	7, 8
BL-4C	2	Flat Double Crystal Si (111)	Bent Cylinder	6 ~ 21	0.7×0.5		~5	9, 10
BL-6A	1.2	Bent Si(111) (α = 0°, 6.0°, 7.8°, 9.5°, 11.4°, 13.7°, 16.5°)	Bent Plane Fused Quartz	5 ~ 25	2.5×1			11
BL-6B	1	Bent Si(111)	Bent Plane Si Pt-coated		1.7×0.2			12
BL-6C	2	Bent Si (111)	Bent Plane Si Pt-coated					13
BL-7C	4	Double Crystal Si (111) Sagittal Focusing	Double Mirror Fused Quartz Focusing	4 ~ 20 (4 ~ 13)	5×1	1×10^{10}/6mm^2 (8 keV, 300 mA) (1×10^{11} when focused)	~ 2	14 - 16
BL-8C	5	Channel-Cut Si(220), Si(111), Si(400)	None	5 ~ 40	50×5	6×10^{8}/mm^2 (10 keV, 300 mA)	~2	
BL-9A	3	Double Crystal Si (111)	Collimating and Focusing Bent Conical Mirrors (Rh Coated) Double Flat Mirror (Rh/Ni Coated)	2.2 ~ 15	1×0.3	4×10^{11}(9 keV, 300 mA)	2	17, 18
BL-9C	3.5	Double Crystal Si(111)	Bent Cylinder Rh-coated Si	4 ~ 23 or white	1×1	5×10^{10}(9 keV, 300 mA)	~ 2	

Branch Beamline	Horizontal Acceptance (mrad)	Type of Monochromator	Mirror	Photon Energy (keV)	Beam Size (H×V) (mm)	Photon Flux at Sample Position (/s)	Energy Resolution ($\Delta E/E \times 10^{-4}$)	Reference
BL-10A	1	Si(111), Si(311) Quartz(100), PG(002) Curved Si(111) (α~ 4°, 8°)	Plane Pt coated Fuzed Quartz	5 ~ 25	10×3		10 ~ 5	19
BL-10B	2	Channel-Cut Si(311)	None	6 ~ 30	5×1	1×10^{9}/7mm^2	1	
BL-10C	4	Double Crystal Si(111)	Bent Cylinder	4 ~ 10	1.2×0.2	~10^{11}/1.5mm^2 (8 keV, 400 mA)	2	
BL-12C	2	Double Crystal Si(111) Si(311)	Bent Cylinder	6 ~ 23	0.65×0.4	5×10^{10}/1mm^2 (8 keV, 300mA) w.Si(111)	~ 2	20
BL-13A	1	Double Crystal Si(111), Ge(111)	Cylinder Pt-coat Fused Quartz	30	0.045×0.032	5×10^{10}/1mm^2	~ 2	21
BL-13B1 B2	4	Double Crystal Si(111), Si(220) Sagittal Focusing	Bent Plane Fused Quartz	4 ~ 30	4×1		~ 2	22
BL-14A	1.28 (Vertical)	Double Crystal Si (111) Si (311) Si (553)	Bent Cylinder Pt-coated Fused Quartz	5.1 ~ 19.1 9.9 ~ 35.6 22.7 ~ 84.5	2×1 at focus 5×38		2	23
BL-14B	2.2 (Vertical)	Double Crystal Si(111),	None	10 ~ 57	5×14		2	
BL-14C1 C2	1.3 (Vertical)	Double Crystal Si(111), Si(220)	None	5 ~ 100 or white	6×35		2	24, 25
BL-15A	2	Bent Crystal Ge(111) (α = 8.0°)	Bent Plane, Fused Quartz Pt-coated	8.0 (fixed)	0.5×0.25	9×10^{10}/mm^2 (8.0 keV, 350 mA)	~ 10	26
BL-15B1 B2	2	Double Crystal Si (111)	Bent Cylinder	5 ~ 20 or white	0.6×0.4	10^{11}/1mm^2 (8.0keV, 350mA)	~ 2	
BL-15C	2	Double Crystal Si (111)	None	4 ~ 30	60×6			
BL-16A1 A2	1	Double Crystal Si(111) Sagittal Focusing	Bent Plane (Ph on Si) and Bent Plane (Rh on SiC)	4 ~ 25	1.2×0.5	~1×10^{13} (8.3 keV, 300 mA)	~ 1	27
BL-17A	4	Double Crystal Si(111)	None	5 ~ 13	100×10		~ 2	28
BL-17C	1	Double Crystal Si(111)	None	5 ~ 13	20×5		~ 2	29

Branch Beamline	Horizontal Acceptance (mrad)	Type of Monochromator	Mirror	Photon Energy (keV)	Beam Size (H×V) (mm)	Photon Flux at Sample Position (/s)	Energy Resolution ($\Delta E/E$)×10^{-4}	Reference
BL-18B	2	Double Crystal Si(111) Si(220) Ge(111) Ge(220)	Bent Cylinder Fused Quartz, Pt-coated	6 ~ 30	0.6×0.4	1.1×10^{10} (12.4 keV, 300 mA) Si(111)	~ 2	30
BL-18C	1	Double Crystal Si(111)	Cylinder Fused Quartz, Pt-coated	6 ~ 25	0.07×0.04		~2	
BL-20B	2	Channel Cut Si(111) Double Crystal Sagittal focusing Si(111)	None	4 ~ 25	26×3		~ 2	31
BL-27B	4	Double Crystal Si(111)	None	4 ~ 20	100×6		~ 2	32
BL-28B	H: 4 V:0.2	Double Crystal Si(111) Si(220) InSb(111)	Pre-mirror Bent Cylinder Si Pt- & Ni-coated Post-mirror Bent Plane Fused Quartz Pt- & Ni-coated	2 ~ 10	2.0×0.2	3×10^{10} (9 keV, 300mA Si(220) Pc ~ 0.5)	~ 2 (Si(111))	33
AR-NE1A1	2	Double Bent Crystal Si(111) Si(400)		40 ~ 70 80 ~ 160	2×0.5	2×10^{13} (60 keV, 35mA)	8	34 - 36
AR-NE1A2	2	Asym. cut Single Crystal Si(311)		33 ~ 38	75×120 ~140	10^{10}(33 keV)	60	
AR-NE3	H:0.3 V:0.03	Double Crystal Si(111) High-resolution Monochromator Nuclear Monochromator of Single Crystal $^{57}Fe_2O_3$(777)		5 ~ 25 8 ~ 26 14.4	15×2	 1×10^{3} (14.4 keV)	1 5×10^{-3} 1×10^{-7}	37
AR-NE5A	10	Asym.Cut Single Crystal Si(311), Si(511) (α= 4° ~ 6°) Double Crystal Si(311), Si(111), Si(220)		20 ~ 60 20 ~ 100	150×80 100×3	5×10^{8} (33.2 keV)	60 2	38, 39
AR-NE5C	3	Double Crystal Si(111)	None	30 ~ 100 or white	60×5		5	40

References

[1] A. Fujiwara *et al.*, *J. Appl. Cryst.* **33** (2000) 1241.
[2] S. Sasaki *et al.*, *Rev. Sci. Instrum.* **63** (1992) 1047.
[3] K. Kawasaki *et al.*, *Rev. Sci. Instrum.* **63** (1992) 1023.
[4] T. Mori and S. Sasaki, *Rev. Sci. Instrum.* **66** (1995) 2171.
[5] A. Iida *et al.*, *Rev. Sci. Instrum.* **66** (1995) 1373.
[6] K. Ohsumi *et al.*, *Rev. Sci. Instrum.* **66** (1995) 1448.
[7] Powder Diffraction User Group, *KEK Report* **94-11** (1995).
[8] H. Toraya, H. Hibino and K. Ohsumi, *J. Synchrotron Rad.* **3** (1996) 75.
[9] H. Iwasaki *et al.*, *Rev. Sci. Instum.* **60** (1989) 2406.
[10] *Photon Factory Activity Report* **1995 #13** (1996) E-1.
[11] N. Sakabe et al., *Rev. Sci. Instrum.* **66** (1995) 1276.
[12] *Photon Factory Activity Report* **1995 #13** (1996) C-1.
[13] N. Sakabe et al., *Nucl. Insrtum. Meth.* **A467-468** (2001) 1367.
[14] M. Nomura and A.Koyama, *KEK Internal* **93-1** (1993).
[15] M. Nomura et al., *KEK Report* **91-1** (1991).
[16] M. Nomura and A. Koyama, in *"X-ray Absorption Fine Structure"*, ed. by S. S. Hasnain, Ellis Horwood, Chichester, 1991, p.667.
[17] M. Nomura and A. Koyama, *J. Synchrotron Rad.* **6** (1999) 182.
[18] M. Nomura and A. Koyama, *Nucl. Insrtum. Meth.* **A467-468** (2001) 733.
[19] S. Sasaki, *Rev. Sci. Instrum.* **60** (1989) 2417.
[20] M. Nomura and A. Koyama, *KEK Report* **95-15** (1996).
[21] *Photon Factory Activity Report* **2000 #18** (2001) A.
[22] *Photon Factory Activity Report* **1994 #12** (1995) C-6.
[23] Y. Satow and Y. Iitaka, *Rev. Sci. Instrum.* **60** (1989) 2390.
[24] *Photon Factory Activity Report* **1999 #17** (2000) A 92.
[25] *Photon Factory Activity Report* **1999 #17** (2000) A 103
[26] Y. Amemiya *et al.*, *Nucl. Instrum. Meth.* **208** (1983) 471.
[27] *Photon Factory Activity Report* **1994 #12** (1995) E-3.
[28] *Photon Factory Activity Report* **1988 #6** (1988) I-15.
[29] Y. Horii *et al.*, *Rev. Sci. Instrum.* **66** (1995) 1370.
[30] N. Watanabe *et al.*, *Rev. Sci. Instrum.* **66** (1995) 1824.
[31] R.F. Garret *et al.*, *Rev. Sci. Instrum.* **66** (1995) 1351.
[32] H. Konishi *et al.*, *Nucl. Insrtum. Meth.* **A372** (1996) 322.
[33] T. Iwazumi *et al.*, *Rev. Sci. Instrum.* **66** (1995) 1691.
[34] H. Kawata *et al.*, *Rev. Sci. Instrum.* **60** (1989) 1885.
[35] H. Kawata *et al.*, *J. Synchrotron Rad.* **5** (1998) 673.
[36] H. Kawata *et al.*, *Nucl. Insrtum. Meth.* **A467-468** (2001) 404.
[37] X. Zhang *et al.*, *Rev. Sci. Instrum.* **63** (1992) 404.
[38] K. Hyodo *et al.*, *Handbook on SR* **IV**, (1991) 55.
[39] Y. Itai *et al.*, *Rev. Sci. Instrum.* **66** (1995) 1385.
[40] T. Kikegawa *et al.*, *Rev. Sci. Instrum.* **66** (1995) 1335.

Table 4 VUV and Soft X-ray Beamline Optics.

Branch Beamline	Acceptance Hor. & Ver. (mrad)	Type of Monochromator	Grating Groove Density (l/mm)	Photon Energy (eV)	Beam Size (mm)	Typical Resolving Power (E/ΔE) and Photon Flux (/s)	Reference
BL-1C	5 3	Varied-Space Plane Grating	300 600 1200	20 ~ 60 40 ~ 120 80 ~ 240	1 × 1	1000 ~ 10000 10^{11} ~ 10^{9}	1
BL-2A Undulator	K = 0.5 ~ 2.2 λu = 6 cm	Double Crystal InSb (111), Si (111)	____	1740 ~ 5000	< 1ϕ	2000, 8000 10^{11}	2 - 5
BL-2C Undulator	K = 0.55 ~ 2.2 λu = 6 cm	Varied-Space Plane Grating	1000 2200	250 ~ 1400	0.9 × 0.1	5000 ~ 10000 10^{11} ~ 10^{10}	6 - 8
BL-3B	10 2	Grazing Incidence R = 24 m α+β = 165°	200 600 1800 150	10 ~ 280	< 2ϕ	200 ~ 3000 10^{12} ~ 10^{9}	9, 10
BL-7A (RCS)	6 1	Varied-Line-Space Plane Grating	300 650	50 ~ 1500	2.5 × 0.5	1000 ~ 9000 10^{12} ~ 10^{9}	
BL-7B (RCS)	6 4	1m Seya-Namioka	1200 2400	5 ~ 50	1 × 1	1000	11
BL-8A (Hitachi)	0.5 1	SX700 Plane Grating	1221	38 ~ 2300	5 × 1	2000 10^{10}	
BL-8B (Hitachi)	3 0.5	Double Crystal InSb (111), Si (311)	____	1700 ~ 14000	1.9 × 0.5	5000	12
BL-11A	5 1	Varied-Line-Space Plane Grating	300 800 1200	70 ~ 1900	2 × 1	500 ~ 5000 10^{12} ~ 10^{9}	13 - 16
BL-11B	4 0.6	Double Crystal InSb (111), Ge (111)	____	1760 ~ 3910	5 × 2	2000 10^{10}	4, 17, 18
BL-11C	4.8 3	1m Seya-Namioka	1200	4 ~ 35	~1ϕ	1000	19
BL-11D	4 2	Varied-deviation angle-type Grazing Incidence On-blaze Mount R_1 = 52.5 m R_3 = 22.5 m	2400	G_3 60 ~ 245 G_1 200 ~ 900	1 × 0.1	2000 10^{11}	20
BL-12A	2.2 0.34	Grazing Incidence R = 2 m α = 88°	1200	30 ~ 1000	2 × 3	1000 10^{9}	21
BL-12B	5 3.6	6.65 m Off-Plane Eagle	1200 4800	5 ~ 30	____	2.5 × 10^{5} 10^{4}	22 - 24
BL-13C Undulator	K = 0.3 ~ 4.2 λu = 18 cm	Grazing Incidence R = 50 m α+β = 173.2°	350 750	70 ~ 500 150 ~ 1000	5 × 1	1000 ~ 6000 10^{12} ~ 10^{10}	25, 26

Branch Beamline	Acceptance Hor. & Ver. (mrad)	Type of Monochromator	Grating Groove Density (l/mm)	Photon Energy (eV)	Beam Size (mm)	Typical Resolving Power (E/ΔE) and Photon Flux (/s)	Reference
BL-16B Undulator	K = 0.5 ~ 5.75 λu = 12 cm	Grazing Incidence R = 24 m α+β = 168.6°	400 900 2000	40 ~ 550	< 1φ	1000 ~ 10000 10^{12} ~ 10^{10}	27 - 29
BL-17B (Fujitsu)	8 1	Toroidal Mirror	____	____	10 × 1	____	____
BL-18A (ISSP)	2 2	Grazing Incidence R = 3 m α+β = 160° R = 6.65 m α+β = 167.5°	300 600 1200 500	15 ~ 150	< 1φ	1000~2000 10^{11} ~10^{9}	30
BL-19A Revolver Undulator (ISSP)	K = 1.0 ~ 9.0 λu = 16.4 cm K = 0.5 ~ 1.25 λu = 5 cm K = 0.5 ~ 2.5 λu = 7.2 cm K = 1.0 ~ 5.0 λu = 10 cm	Grazing Incidence R = 2 m α+β = 160° R = 4 m α+β = 170°	600 1200 600 1200	12 ~ 250	< 0.7φ	1000 10^{12}	31, 32
BL-19B Revolver Undulator (ISSP)		Varied-space Plane Grating	800 2400	10 ~ 1200	< 0.5φ	400~4000 10^{12} ~10^{11}	32 - 34
BL-20A	28 5	3m Normal Incidence	1200 2400	5 ~ 40	2 × 1	300 ~ 30000 10^{12} ~ 10^{8}	35
BL-27A	5 0.5	Double Crystal InSb (111)	____	1800 ~ 4000		2000	36
BL-28A Helical Undulator	K_x = 0.23 ~ 3 K_y = 0.23 ~ 6 λu = 16 cm	Grazing Incidence R = 2 m α+β = 160° R = 4 m α+β = 170°	600 1200 600 1200	30 ~ 250	< 0.5φ	1000 10^{10}	37
AR-NE1B Helical Undulator	K_x = 0.2 ~ 3 K_y = 0.2 ~ 6 λu = 16 cm	Grazing Incidence R = 10m β = 89°	1200 2400	250 ~ 1800	~0.8 × 0.2	1000~5000 10^{11} ~10^{9}	38, 39

References

[1] K. Ono *et al.*, *Nucl. Instrum. Meth.* **A467-468** (2001) 573.
[2] H. Maezawa *et al.*, *Nucl. Instrum. Meth.* **A246** (1986) 310.
[3] Y. Kitajima *et al.*, *Rev. Sci. Instrum.* **63** (1992) 886.
[4] Y. Kitajima, *J. Elec. Spec. Relat. Phenom.* **80** (1996) 405.
[5] Y. Kitajima, *J. Synchrotron Rad.* **6** (1999) 167.
[6] Y. Yan and A. Yagishita, *KEK Report* **95-9** (1995) .
[7] M. Watanabe *et al.*, *Proc. SPIE* Vol. **3150** (1997) 58.
[8] M. Watanabe *et al.*, *Nucl. Instrum. Meth.* **A467-468** (2001) 512.
[9] A. Yagishita *et al.*, *Nucl. Instrum. Meth.* **A306** (1991) 578.
[10] S. Masui *et al.*, *Rev. Sci. Instrum.* **63** (1992) 1330.
[11] H. Namba *et al.*, *Rev. Sci. Instrum.* **60** (1989) 1917.
[12] K. Ogata *et al.*, *Photon Factory Activity Report* **1994 #12** (1995) 164.
[13] K. Amemiya *et al.*, *J. Synchrotron Rad.* **3** (1996) 282.
[14] K. Amemiya *et al.*, *Proc. SPIE Proceedings* **3150** (1997) 171.
[15] Y. Kitajima *et al.*, *J. Syncrotron Rad.* **5** (1998) 729.
[16] Y. Kitajima *et al.*, *J. Elec. Spectrosc. Relat. Phenom.* **101-103** (1999) 927.
[17] T. Ohta *et al.*, *Nucl. Instrum. Meth.* **A246** (1986) 373.
[18] M. Funabashi *et al.*, *Rev. Sci. Instrum.* **60** (1989) 1983.
[19] *Photon Factory Activity Report* **1982/1983** (1984) V-15.
[20] *Photon Factory Activity Report* **1997 #15** (1998) A 101.
[21] *Photon Factory Activity Report* **1992 #10** (1993) I-2.
[22] K. Ito *et al.*, *Appl. Opt.* **25** (1986) 837.
[23] K. Ito *et al.*, *Appl. Opt.* **28** (1989) 1813.
[24] K. Ito and T. Namioka, *Rev. Sci. Instrum.* **60** (1989) 1573.
[25] N. Matsubayashi *et al.*, *Rev. Sci. Instrum.* **63** (1992) 1363.
[26] H. Shimada *et al.*, *Rev. Sci. Instrum.* **66** (1995) 1780.
[27] E. Shigemasa *et al.*, *KEK Report* **95-2** (1995) .
[28] *Photon Factory Activity Report* **1995 #13** (1996) E-2.
[29] E. Shigemasa *et al.*, *J. Synchrotron Rad.* **5** (1998) 777.
[30] S. Suzuki *et al.*, *Activity Report of SRL-ISSP* **60** (1989) .
[31] A. Kakizaki *et al.*, *Rev. Sci. Instrum.* **60** (1989) 1893.
[32] A. Kakizaki *et al.*, *Rev. Sci. Instrum.* **63** (1992) 367.
[33] M. Fujisawa *et al.*, *Nucl. Instrum. Meth.* **A467-468** (2001) 309.
[34] M. Fujisawa *et al.*, *Nucl. Instrum. Meth.* **A467-468** (2001) 313.
[35] K. Ito *et al.*, *Rev. Sci. Instrum.* **66** (1995) 2119.
[36] H. Konishi *et al.*, *Nucl. Instrum. Meth.* **A372** (1996) 322.
[37] Y. Kagoshima *et al.*, *Rev. Sci. Instrum.* **63** (1992) 1289.
[38] Y. Kagoshima *et al.*, *Rev. Sci. Insturm.* **66** (1995) 1696.
[39] Y. Kagoshima *et al.*, *Rev. Sci. Instrum.* **66** (1995) 1534.

2 Reconstruction and Upgrading of Beamlines

2-1 BL-1A, Crystal Structure Analysis Beamline of "Collaboratory"

BL-1A was constructed as a joint project based on the following two proposals: a proposal for a “Study on correlated electron systems by a new research network” and a proposal for the “Crystal structure analysis of strongly correlated electron systems”. The former proposal is being conducted by five institutes: Institute of Materials Structure Science, Institute for Materials Research, the Institute for Solid State Physics, Institute for Molecular Science, and Institute for Chemical Research Kyoto University. The latter proposal is being conducted by the Correlated Electron Research Center.

The aim of the former proposal is to make a new research field between material physics and material chemistry by using a new research network, which is called “collaboratory”. The collaboratory is a new network system to realize close coupling among researchers in different fields and to supply them with easy utilization of the experimental apparatus in remote facilities. The two-dimensional warped imaging plate diffractometer (Rigaku) have been installed for this purpose. The aim of the latter proposal is to precisely analyze the crystal structure of materials for new electronic devices and to elucidate the mechanism of the functions in strongly correlated systems. Not only a conventional diffraction experiments, but also a special technique, like resonant X-ray scattering experiments, can be made on this diffractometer to study the electronic states in crystals. A seven circles diffractometer (7C-XRD, Huber) and a diamond phase shifter have been installed for this purpose (Figs. 1 and 2).

In this beamline, X-rays are monochromatized by Si (111) double crystals and focused by a cylindrical bent mirror. 7C-XRD and the optical devices are controlled by a spec-GPIB system installed on a PC (Linux), and after the first emitted light had been induced in December 2001, the best setup of optical system has been worked out. The size of the tuned photon beam is 0.3 mm (vertical direction) × 0.7 mm (horizontal direction), and the deviation of the center position is only 0.2 mm (vertical direction) during changing the energy from 5 to 20 keV. It was found that the intensity of the photon beam is 4×10^{11} cts/sec at 8 keV, ring current $I = 400$ mA.

Since March 2002, the machine time has been spent on the setup of the diffractometers, equipment and environmental considerations such as IP, He-path, noise-cut housings. To provide the sample environments with a wide temperature range, the cryojet system (Oxford Instruments, $T = 80$ K - 400 K) and the low temperature cryostat (Daikin, T > 10 K) are now available. A cryostat equipped with a diamond anvil cell (DAC), oriented to

Figure 1
Experimental hutch and operation area at BL-1A.

Figure 2
Seven circles diffractometer (7C-XRD, Huber, backward) and imaging plate diffractometer (Rigaku, front) equipped in BL-1A.

high pressure and low temperature experiments, will be installed in the near future. Above the hutch, a sample preparation table is furnished with a microscope (Nikon co.) and a workstation for data analysis. Users can check the condition inside the hutch during the experiments by watching the monitor window in the web site (http://pfwww.kek.jp/beamlines/bl-1a/webcam.html).

2-2 BL-9C, New Apparatus for Small- and Wide-Angle Scattering Experiments

BL-9C was reconstructed to realize the small angle scattering (SAXS) experiments in 2000 [1], and consists of a Si(111) double crystal monochromator and a focusing bent cylindrical mirror. The focus size is 0.5 x 1.1 mm^2 at the detector position (29.67 m). A pair of slits, at 21 m and in the experimental hutch (at 28.2 m), determine the resolution in small-angle region.

The new apparatus is designed to realize SAXS and wide-angle scattering (WAXS) experiments with differential scanning calorimetry (DSC) and depolarized small-angle light scattering (Hv-SALS) simultaneously. Simultaneous measurements which observe a variety of length scales help us understand formation of hierarchical structures of soft materials, such as crystalline polymers (crystalline homopolymer, block copolymer, and polymer blend) and lipids (phospho lipid, cholesterol, fatty acid, fats, wax, etc.). For example, crystalline polymers form hierarchical structures, consisting of crystals with periodicity on the angstrom scale, the periodical structures of these crystals and amorphous regions with the periodicity on nanometer scale, and the micrometer-scale spherulites. The formation of the hierarchical structures involves observation of the development of these structures on quite different length scales. In order to elucidate the mechanism of structural formation, we have long needed an apparatus that can observe structure on a variety of length scales simultaneously.

A schematic illustration of the apparatus is shown in Fig. 3. A vacuum chamber for SAXS and WAXS was employed to reduce background scattering and absorption due to air. The equipment for the Hv-SALS measurement, such as mirrors, polarizer, analyzer and laser can be set as shown in Fig. 3. In order to perform the simultaneous SAXS/ WAXS/ DSC measurement, the DSC equipment (Mettler FP90) can be set at the sample position. Typical q-ranges attainable for SAXS and WAXS are $0.1 < q < 3.0$ and $11 < q < 22$ nm^{-1}, respectively. Here $q = (4\pi/\lambda)\sin(\theta/2)$, and λ and θ are the wavelength of the X-ray beam, typically 0.1499 nm, and the scattering angle, respectively.

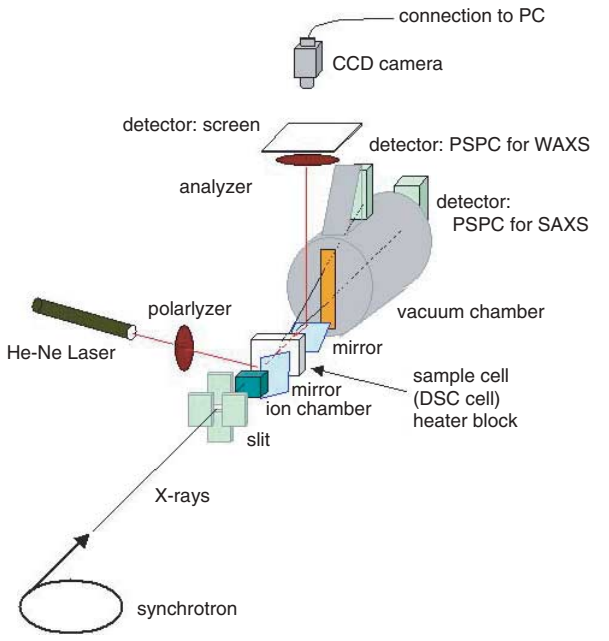

Figure 3
Schematic illustration of the simultaneous SAXS/ WAXS/ Hv-SALS measurement apparatus.

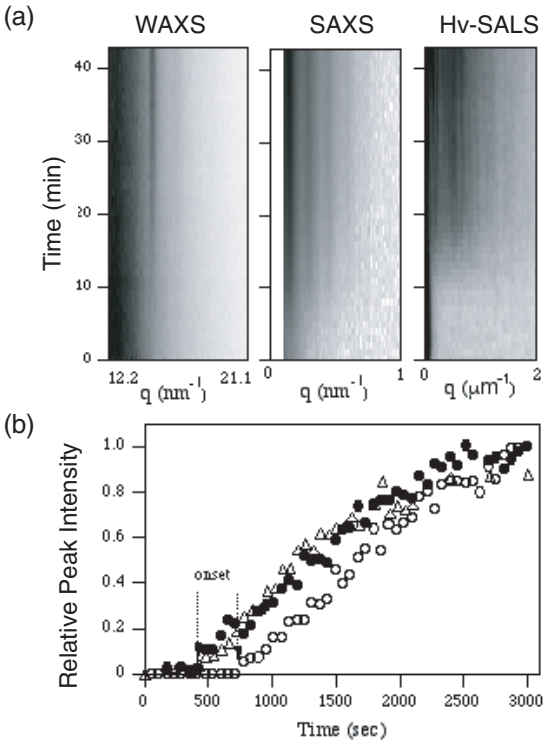

Figure 4
(a) Temporal Change of WAXS (left), SAXS (middle), and Hv-SALS (right). Darker region shows the higher intensity. (b) Relative peak intensity change as a function of time. Open circles, closed circles and open triangles indicate WAXS, SAXS and Hv-SALS, respectively.

As a model of hierarchical structure, we studied the crystallization kinetics of crystalline-amorphous block copolymers in order to demonstrate the performance of the new apparatus [2–4]. The specimen used was a crystalline-amorphous block copolymer comprising

hydrogenated polybutadiene and hydrogenated polyisoprene. The specimen was annealed at 180˚C and successively cooled down to 103˚C (slightly below its melting point, i.e., ca. 110˚C) at a rate of 30 deg/min. Figure 4(a) shows the temporal change of WAXS, SAXS and Hv-SALS in the left, middle and right parts, respectively. The vertical axis is the time. In Fig. 4(b), the increase of the peak intensity observed in WAXS, SAXS and Hv-SALS during the crystallization is compared as a function of time. Interestingly, it was found that Hv-SALS intensity started to increase almost simultaneously with SAXS but prior to WAXS. These early changes in Hv-SALS and SAXS suggest that the formation of spherulite and the formation of the long-periodic structure of the crystalline and the amorphous regions took place in the early stage. In other words, the precursory density fluctuation of the length scale of nanometer and micrometer was formed prior to crystallization of the crystalline polymer chains on the order of angstrom during the nucleation and the growth process. These successful experimental results proved the potential of BL-9C for the use of simultaneous time-resolved SAXS and WAXS measurement with SALS and DSC.

References

[1] *Photon Factory Activity Report* **2000 #18** (2001) A 71.
[2] S. Okamoto, K. Yamamoto *et al.*, *XII International Conference on Small-Angle Scattering 2002 preprint*, pp. 152, 2002.
[3] S. Okamoto, K. Yamamoto *et al.*, Synchrotron Radiation in *Polymer Science II preprint*, pp. 52, 2002.
[4] K. Yamamoto, S. Okamoto *et al.*, *Photon Factory Activity Report* **2001 #19** (2002) B 177.

2-3 Present Status of the PF-AR

1. Outline

Figure 5 shows the top view of the present PF-AR experimental halls and beamlines. As described in the preceding volume of the Activity Report, a second supplemental budget was approved in 2000 for the construction of a new experimental hall (NW-Experimental hall), as well as a new X-ray undulator beamline (NW12) for protein crystallography. At the beginning of January 2002, the commissioning of the PF-AR accelerator started, and we could get a first beam from the X-ray undurator beamline (NW2), which was constructed as a dedicated beamline for XAFS experiment, especially for time-resolved experiments. At the end of March 2002, the construction of the NW-Experimental hall was completed. The alignment of the beamline component for NW12 and also the user machine time started at the beginning of April 2002.

2. NW-experimental hall

The NW-experimental hall building was constructed for two insertion device beamlines (NW12 and NW14) and two bending magnet beamlines (NW8 and NW10) as shown in Fig. 5. The experimental hall is located under ground level. There are several preparation rooms for sample, detector, vacuum system, and data processing, at the same level as the experimental hall. At the ground level, there are: a resting room for users, a room for chemical treatment of samples, and an entrance. Figure 6 shows the entrance to the NW-experimental hall building.

3. Present status of AR-NW2 (XAFS beamline)

The detailed design of the beamline was described in the preceding volume of the Activity Report [1]. The first beam of the undulator was observed on February 4, 2002. Then, we progressed to commission the monochromator and mirror system.

The double crystal monochromator consists of flat silicon (111) crystals, which are cooled by liquid nitrogen in order to reduce the deformation caused by the heat load. One of the characteristic points of the monochromator is the usage of a relatively long second silicon crystal (~200 mm long) along the beam direction. The long crystal makes it possible to reduce the mechanical translation stage for the second crystal, which is needed to realize the fixed exit position for the monochromatized X-rays, because the perfection of the crystal itself can be used as a good translation stage. We introduced a circulation system of liquid nitrogen, which was developed by T. Mochizuki *et al.* [2] at SPring-8. The system can handle the incoming heat power upto about 330 W. Figure 7 shows the rocking curves of Si (111)(11.39 keV) and (333)(34.17 keV) diffractions at the condition of the minimum gap of the undulator (10 mm), which corresponds to K=3. The total radiation power on the monochromator crystal was about 300 W. As shown in this figure, the width of the (333) diffraction was less than 1 arcsec, and we could not observe any heat load problem. The condition of the fixed exit position could be adjusted by the Bragg angle dependence of the first crystal height position. After adjusting the several parameters, it is possible to keep the deviation of the beam position at the experimental hutch less than 0.1 mm in both horizontal and vertical directions scanning the monochromatized energy from 5 to 25 keV.

Several spectra of the undulator synchrotron radiation at different K-values have been observed. As described in the preceding volume of the Activity Report, the undulator of this beamline has optional mechanics to make a tapered undulator in order to obtain a relatively wider energy spread ($\Delta E/E \sim 10^{-1}$) of the 3rd harmonics for the Dispersive XAFS experiments. Figure 8 shows the taper dependence of the spectrum on 3rd harmonics undulator synchrotron radiation, whose K-value is equal to 1.5. The energy spread of the 3rd harmonics is about 300 eV in the case of the normal undulator (taper=0.0 mm). On introducing the tapered mode, the shape of the peak becomes flat and its spread becomes wider.

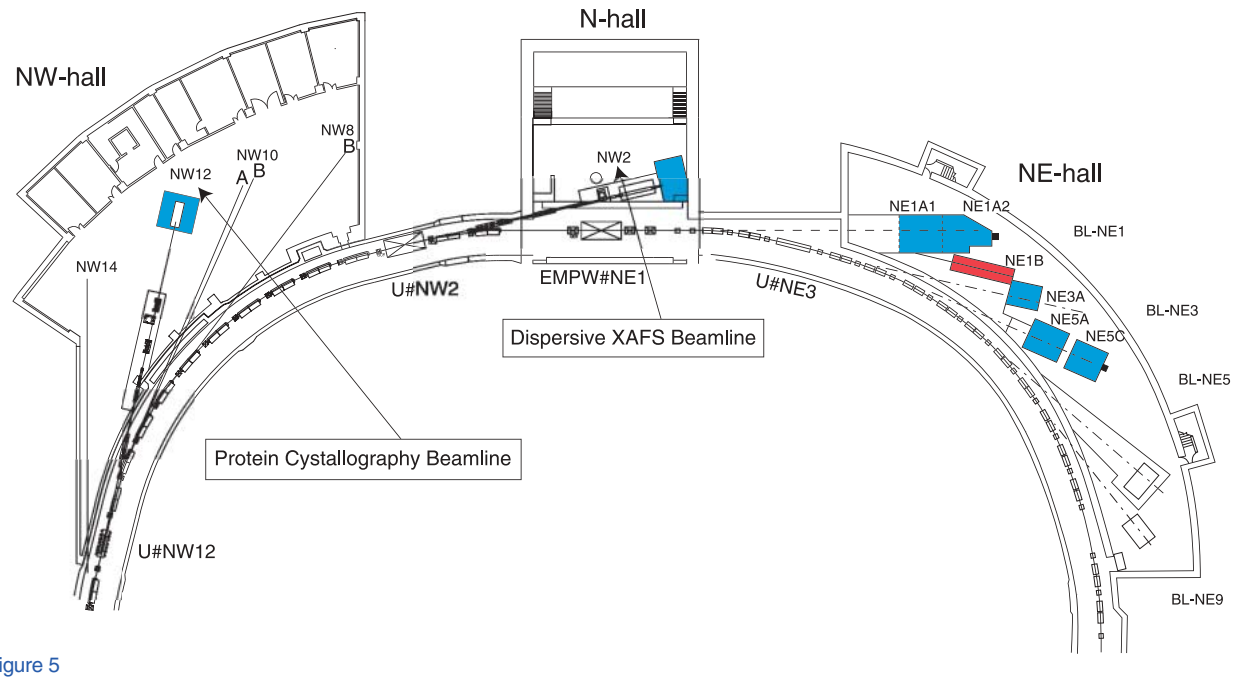

Figure 5
Plan view of PF-AR experimental halls and beamlines. Three beamlines in NE-hall (NE1, NE3, and NE5) have been used for synchrotron radiation experiments and NW2 in N-hall for XAFS experiments has been commissioned and NW12 is under construction in NW-hall.

Figure 6
Entrance of the new NW-experimental hall building.

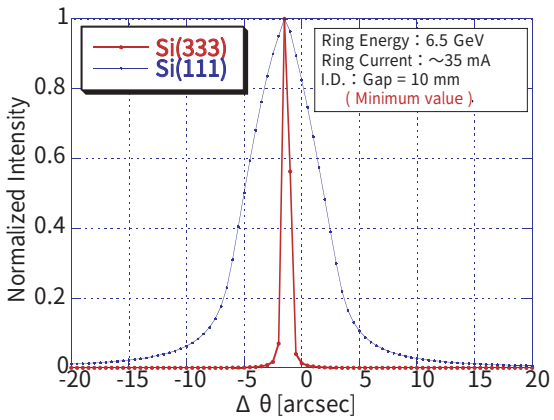

Figure 7
Rocking curves of Si (111)(11.39 keV) and (333)(34.17 keV) diffractions of the double crystal monochromator at the condition of the minimum gap of the undulator 10 mm, which corresponds to K=3. The total radiation power on the monochromator crystal was 300 W. There is no observable heat load problem on the performance of the monochromator.

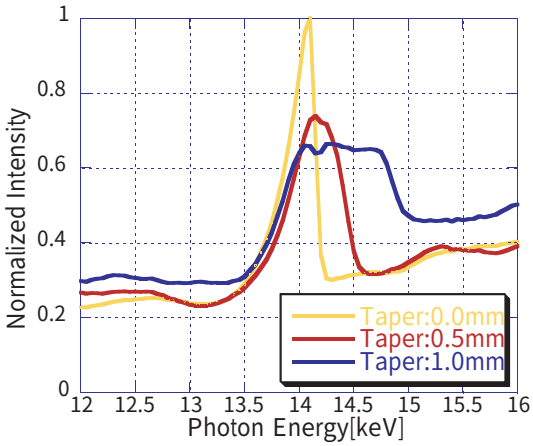

Figure 8
Tapered mode dependence of the spectrum on 3rd harmonics undulator synchrotron radiation, whose K-value is equal to 1.5. The energy spread of the 3rd harmonics is about 300 eV for the case of the normal undulator (taper=0.0mm). On introducing the tapered mode, the shape of the peak becomes flat and the spread becomes wider.

When the tapered angle is set to ~1.0mm/3600mm (Taper =1.0mm in Fig. 8), the energy spread becomes 1 keV. This fact indicates the possibility for doing dispersive XAFS experiments at this beamline.

The focusing mirror system has 4 mirror assemblies; a bent cylindrical mirror for double focusing of X-rays, a flat bent mirror for vertical focusing, and a double-mirror system (cut-off mirrors) to reduce contamination from the higher harmonics. If we want to use a doubly focused beam for high flux XAFS experiment, the bent cylindrical mirror and a double-mirror system will be used. Figure 9 shows the obtained focused beam profiles along the vertical and horizontal directions with the expected ray-tracing calculations. The obtained values of 0.15 mm and 0.45 mm in the vertical and horizontal directions are reasonable as shown in Fig. 9. The double focusing mirror will be replaced by a flat mirror for dispersive XAFS geometry. Then, one of the cut-off mirrors is bent at the meridian direction to make vertical focusing of white X-rays. The preliminary check of the vertical focusing has been done and we obtained a 0.07 mm focused beam at the experimental hutch.

4. Present status of NW12 beamline (Protein crystallography beamline)

The scientific purpose of this beamline is protein crystallography based on the MAD method. The detail of the designing has been described in the preceding volume of the Activity Report. The alignment of the beamline started at the beginning of April 2002 in the NW experimental hall. Figure 10 (a) and (b) show the NW12 beamline in the NW-experimental hall and the mirror adjustment system and monochromator in the main hutch. The commissioning of the beamline component will start at the beginning of October, 2002.

References

[1] *Photon Factory Activity Report* **2000 #18** (2001) A 76.
[2] T. Mochizuki *et al.*, *Nucl. Instrum. Methods*, **A467-8** (2001) 647.

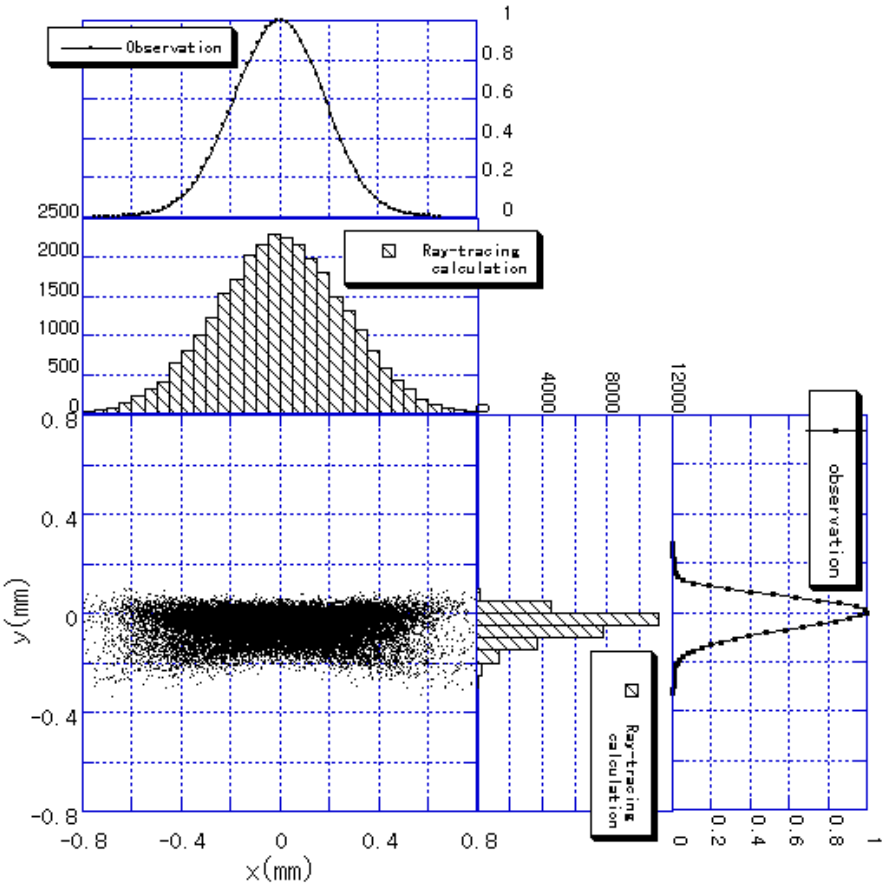

Figure 9
Obtained focused beam profiles along the vertical and horizontal directions with the expected ray-tracing calculations. The obtained values of 0.15 mm and 0.45 mm in the vertical and horizontal directions are reasonable in comparison with the ray-tracing calculations.

(a)

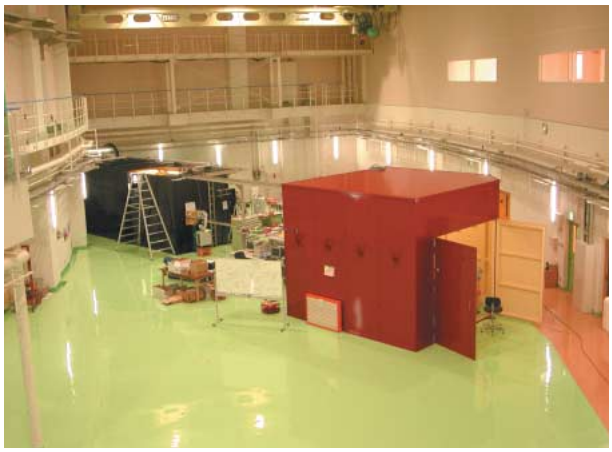

(b)

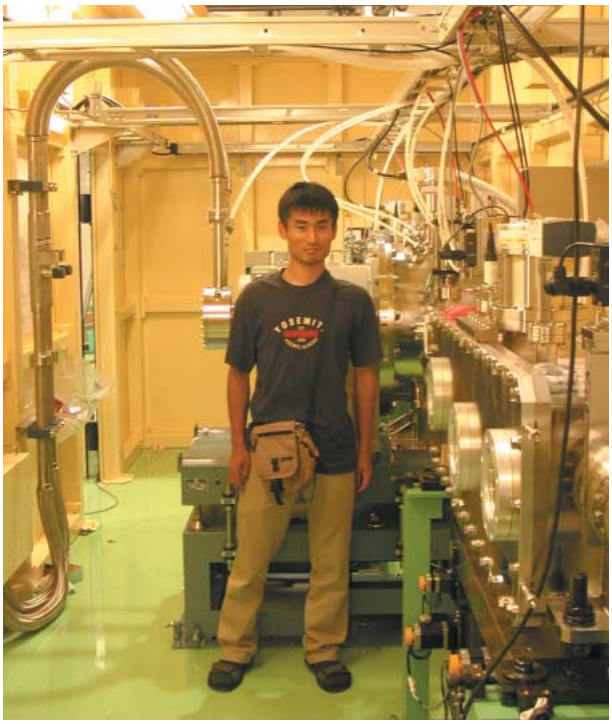

Figure 10
(a) NW12 beamline in the NW-experimental hall and (b) mirror adjustment system and monochromator in the main hutch with Dr. N. Matsugaki who is the responsible of this beamline.

3 New Experimental Facilities and Apparatus

3-1 Slow Positron Facility

In recent years, there has been increasing interest in the use of slow-positron beams (ranging from eV to keV) in various fields of solid state physics. The advantage of utilizing positron beams is in its simpler interactions with matter in contrast to low-energy electrons. For example, the interpretation of low-energy electron diffraction requires extensive computations, whereas that of low-energy positron diffraction is simple owing to the absence of any exchange forces. However, low-energy positron diffraction might not be a practical method due to its poor intensity obtained from a radioactive-isotope-based positron source. An accelerator-based positron source is a good candidate to increase the slow-positron intensity.

Positrons are the antiparticles of the ubiquitous electrons in our world. When in contact, positrons each annihilate with an electron into gamma-rays. In condensed matter, nearly all positrons annihilate with electrons into two gamma quanta. The gamma-rays emerge from the annihilation site in opposite directions. They are modified by the momentum and energy distributions of the electrons in domains of the medium that are sampled by the positron wave function. The annihilation rates are proportional to the electron density in these domains. In this way, positron annihilation experiments can give information about properties of phase space in matter. We can extend these experiments to three dimensions with intense slow-positron beams.

In 2000, we had the water cooling accident of the slow positron generator at KEKB linac tunnel. The linac for the slow positron generator and the slow positron beamline [1] had severe damage. We managed to repair the slow positron beamline from the KEKB linac and perform positronium TOF experiment in FY2000, but the linac for the slow positron generator was in the KEKB linac tunnel and it was very difficult to repair during the operation period of the KEKB linac. A new proposal to reconstruct our linac for slow positron generation from the KEKB linac tunnel to the slow positron experimental hall was presented and acknowledged. We started this reconstruction from the new year shut down period of 2001 [2].

Figure 1 shows the site of the slow positron linac, slow positron generator, slow positron beamline and experimental station in the positron experimental hall on the basement floor of the electron/positron linac building. The dedicated linac and slow positron generator are situated at the north end of the experimental hall. The linac is composed of a conventional thermionic electron gun with extraction voltage of 150 kV and prebuncher, buncher and 4 m accelerator with magnetic lens, quadrupole triplet lens, profile monitors, current monitors and gate valves with evacuation system. There

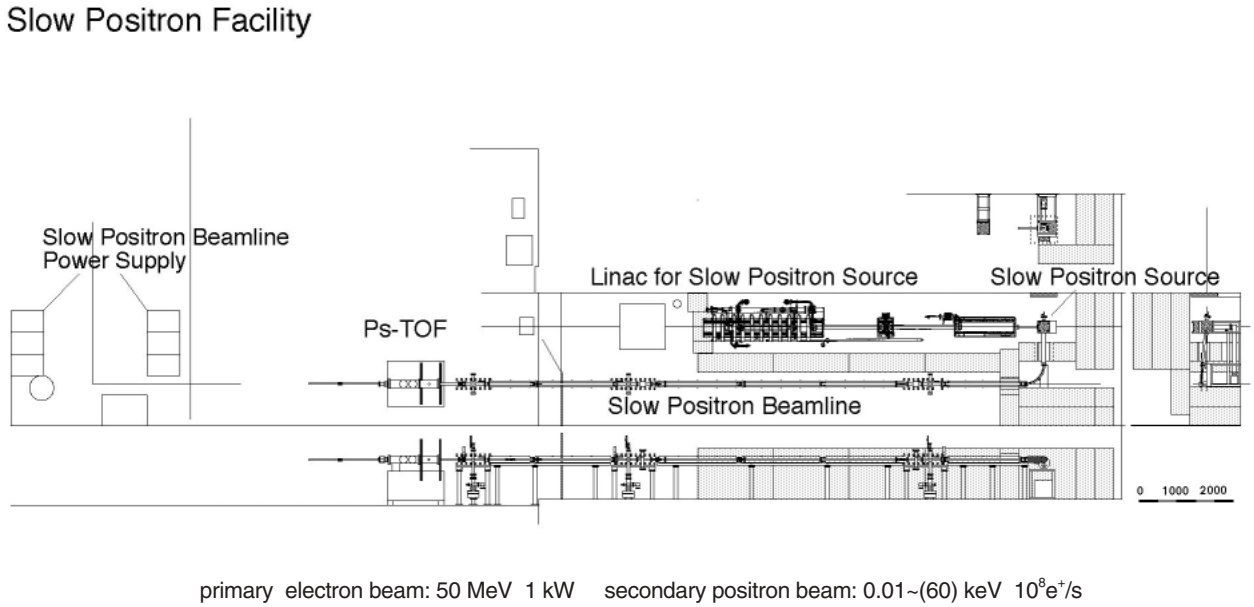

Figure 1
Overview of the new slow positron facility. The 50 MeV electron beam is generated by the linac for the slow positron source. The electron beam is injected into the electron positron converter of the slow positron source. From the moderator assembly mounted behind the electron positron converter, slow positrons are generated and guided through the vacuum duct with the focusing solenoid to the experimental hall.

Table 1 Specifications of the slow positron linac.

Acceleration energy	50 MeV
Beam power	1 kW
Repetition rate	50 Hz
Pulse width	~ ns, μs

Table 2 Specifications of the slow positron beamline.

Positron beam energy	0.01 - (60) keV
Positron beam intensity	10^8 e^+/s
Repetition rate	50 Hz/DC
Energy resolution	NA

are power sources for the electron gun, RF source, controllers for almost all devices for the dedicated linac at the first floor of the experimental hall. The specifications of the slow positron linac are listed in Table 1.

The 50 MeV electron beam is generated by the linac for the slow positron source (Fig. 2). The electron beam is injected into the electron-positron converter of the slow positron source. The vacuum system of the positron source section composed of 60-l/s ion pump and two 400-l/s NEG pumps. The electron-positron converter is mounted on the cold finger of the water cooling system. From the moderator assembly mounted behind the electron positron converter, slow positrons are generated and guided through the vacuum duct with the focusing solenoid to the experimental hall. Solenoids, Helmholtz coils, steering coils are assembled in the Assembly hall, KEK (Fig. 3). There is a 90 degree bending section, three Helmholtz sections and the experimental station. Figure 4 shows the typical Helmholtz section. Monitoring of the slow positron beam is done with this section. The experimental station will be reconstructed in FY 2002. Table 2 gives the specifications of the secondary beamline of this facility .

The slow positron facility will be opened to users in FY2003. The positronium time of flight (Ps-TOF) experimental station will be available. The TOF was determined by measuring the time interval between the arrival time of a pulsed positron beam and the detection of radiated γ-rays from annihilated positronium. Since the lifetime of positronium is well known, we can easily deduce the energy distribution of positronium from the TOF spectra, which were measured by changing the distance between the sample surface and the annihilation γ-ray detector. The positronium work function will be obtained. The surface or the surface related phenomena will be investigated with this experimental station.

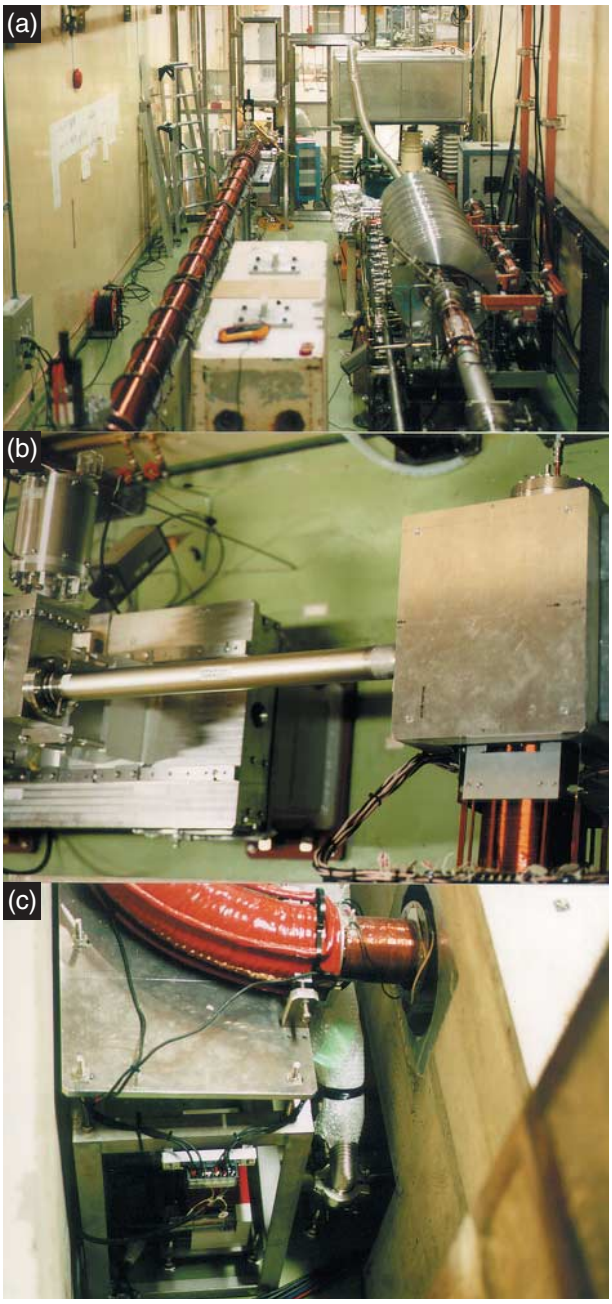

Figure 2
(a) The linac for the slow positron source (right) and the slow positron beamline (left). Both were under construction. After the construction of the linac and the beamline, shield blocks were mounted.
(b) The end part of the linac and the slow positron source. The electron beam comes from the left (south) and the generated slow positron beam goes downward (east).
(c) The 90 degree bending section is situated downstream of the slow positron source. The ion pump of the slow positron source is shown (lower level).

References

[1] T. Kurihara, A. Yagishita, A. Enomoto, H. Kobayashi, T. Shidara, A. Shirakawa, K. Nakahara, H. Saitou, K. Inoue, Y. Nagashima, T. Hyodo, Y. Nagai, M. Hasegawa, Y. Inoue, Y. Kogure, M. Doyama, *Nucl. Instrum. Meth.* **B171** (2000) 164.

[2] T. Kurihara, A. Yagishita, M. Nomura, M. Akemoto, S. Anami, I. Abe, M. Ikeda, A. Enomoto, T. Oogoe, S. Ohsawa, Y. Ogawa, K. Kakihara, A. Katagiri, N. Kamikubota, T. Kamitani, H. Kobayashi, T. Shidara, A. Shirakawa, S. Suwada, K. Nakao, H. Nakajima, S. Fukuda, K. Furukawa, H. Honma, T. Matsumoto, S. Mitizono, Y. Yano, S. Yamaguchi, K. Hosoyama, H. Saito, Y. Nagashima, T. Hyodo, Y. Nagai, M. Hasegawa, M. Inoue, M. Doyama, "*Positron Experiments by using Dedicated Electron Linac", Proc. 26th Linear Accelerator Meeting in Japan, Tsukuba, Japan, Aug 1-3, 2001.*

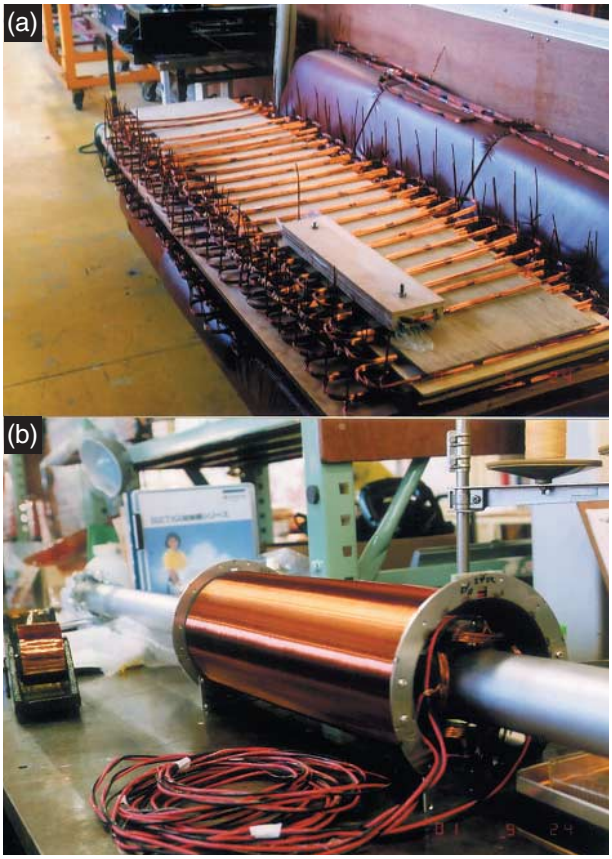

Figure 3
(a) Assembled steering coils are shown.
(b) Prototype of the solenoid, steering coils and a vacuum duct.

Figure 4
The Helmholtz section of the slow positron beamline. From the up stream to downstream, a gate valve, a screen monitor with MCP for the slow positron beam, a CCD camera, an ion pump (60 l/s), an electrode for Penning trap were installed.

3-2 Individual Cell Irradiation System for Radiobiology Using a Microbeam

Risk evaluation of low dose or low dose rate irradiation has been of great concern for human societies utilizing modern technologies. The energy of radiation, after conversion to kinetic energy of secondary charged particles, is deposited in the molecules in the cellular system. The deposited energy to the cell, or dose, is proportional to the number of particle traversing the cell. In the low dose region, the average number of tracks per cell becomes small and hence the numbers show a Poisson distribution. From the characteristics of the Poisson distribution, the fraction of cells that have not accepted any track at all is 37% when the average track number is unity. In the lower dose region, the number of non-hit cells becomes overwhelming against the hit cells. Observation of total cell population without knowing whether each cell is hit or non-hit gives very little knowledge on the mechanisms of cellular response against low dose radiation of environmental circumstances. We need to know if individual cells are irradiated or not in order to study the radiation response of the cell. From this motivation, microbeam irradiation systems using particle (alpha or proton) beams have been developed in the UK [1] and USA [2]. According to recent reports, it was found that a non-hit cell situated nearby an irradiated cell exhibits a certain response to the radiation (bystander effects). This type of response can only be observed when the individual cell is identified and irradiated with a desired amount of dose using a microbeam of about a few microns in diameter.

Considering that we are exposed to γ- or X-ray photons more often than to high energy heavy particles in our living environment, we have planned to develop a microbeam irradiation system using monochromatic synchrotron X-rays in order to study radiation response to low dose X-rays.

Designed system

The proposed system is composed of three parts [3]. The whole system is schematically shown in Fig. 5. First, there is a Karkpatrik-Baez (K-B) mirror system to focus the X-ray beam to the size of 1 μm diameter. Then, the beam is reflected at right angle upwards by a silicon crystal (311), which determines the energy of the X-rays to be 5.35 keV. The range of the photoelectrons generated with the X-rays of this energy is about 0.8 μm. Second, there is a fluorescent microscope equipped with a precise automatic stage, on which the sample dish is fixed and irradiated with the focused X-ray beam from below. The third one is a fluorescence image analyzer (computer) with a sensitive CCD camera, which recognizes the target cells and their positions. This computer also controls irradiation of the X-ray beam to

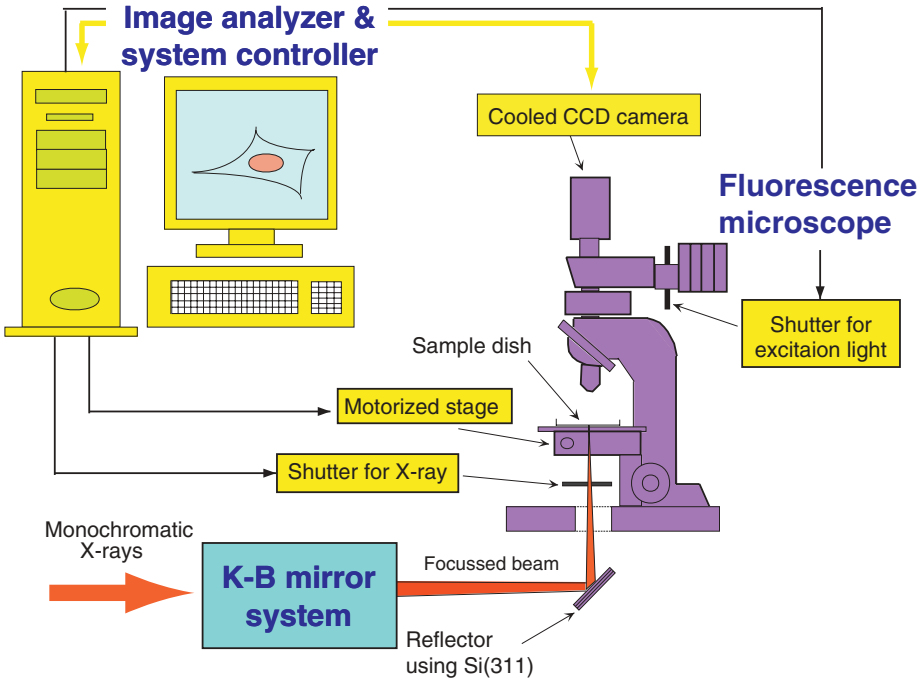

Figure 5
Microbeam irradiation system for radiobiology at Photon Factory.

the target cells, one by one, automatically. The proposed throughput is 1000 cells per hour in order to keep the cells in a good physiological condition during the irradiation process.

This system is planned to be installed at BL-27B in the experimental hall of the 2.5-GeV ring. The experimental stations at BL-27 are situated in the biological sample preparation area, where incubators and other equipment to grow and keep mammalian cells are available.

Preliminary experiments will start in 2003.

References

[1] M. Folkard, B. Vojnovic, K.M. Prise, A.G. Bowey, R.J. Locke, G. Schettino and B.D. Michael, *Int. J. Radiat. Res.* **72** (1997) 375.
[2] C.R. Geard, D.J. Brenner, G. Randers-Pehrson and S.A. Marino, *Nucl. Instrum. Meth.* **B54** (1991) 411.
[3] K. Kobayashi, N. Usami, K. Hieda, K. Takakura, H. Maezawa and T. Hayashi, *Nucl. Instrum. Meth.* **A467-8** (2001) 1329.

3-3 Central Control System for the Beamlines Installed at the PF-AR

At the 2.5-GeV PF Storage Ring, each beamline is equipped with a beamline interlock system (BLIS), to protect the users from radiation hazards and to prevent beamline components from vacuum troubles. The CPU of BLIS is a programmable logic controller (PLC). All the BLISs are connected through optical fiber with a central control system (CCS), which monitors most of the important beamline status and sends, to the beamlines, control signals related to enable/disable of beamline operation. The present CCS in operation at the 2.5-GeV PF Storage Ring was the one renewed in 1999 based on a new concept of "component oriented advanced control kernel", COACK, which has originally been developed as new software for controlling a huge accelerator complex. It is clear that COACK is a very powerful tool not only for controlling accelerators but also for other complicated systems, such as a complex consisting of a CCS and BLISs. COACK has some advantages for our CCS. Firstly, we are able to build virtual beamline images in the COACK server. These images make it possible for users (see Fig. 6) to develop the program to monitor the beamline status and to control the beamlines without any I/O interface board, hardware driver and even real beamline. Secondly, we can avoid a shut down of the system on upgrading programs and editing databases in the PC of clients. In addition, COACK has a big advantage from a budgetary point of view; we need only low price personal computers, and a commonly used network, LAN, to construct the whole system.

In 2001, we have reconstructed a new CCS for the beamlines installed at the PF-AR. There are three separated experimental halls in the PF-AR; three beamlines at the northeast hall (NE-hall), one beamline at the north experimental hall (N-hall), and a new beamline in the northwest hall (NW-hall). This is why we have three CCS in the new system of the PF-AR, as shown in Fig. 7. Each BLIS is directly connected with hard wires to a PLC in the corresponding CCS. Each CCS is equipped with a PC, which is connected with the PLC through RS-

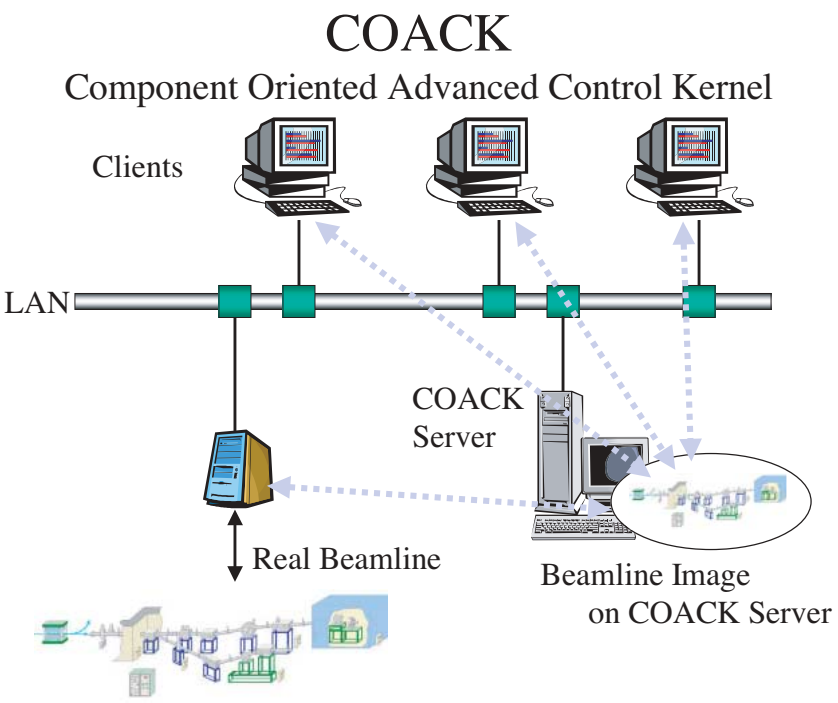

Figure 6
Concept of the beamline image on COACK Server with a LAN.

232C. This PC is included in the COACK control system. Three PLCs are connected to each other with hard wire, and a part of the PLC in the NE-CCS plays the role of head quarter for three CCSs, which sends to the PF-AR Control the ready and safety signals for beam storage and injection, and receives from the Control the beam ready signal for the experiments in each hall.

Note again that all logical judges are carried out in the PLC of each CCS or BLIS of each beamline and the safety is assured with this hard logic system. COACK can make a communication with this system via RS-232C, and can make any order, however, this does not disturb the logic concerning the safety system consisting of a number of PLC.

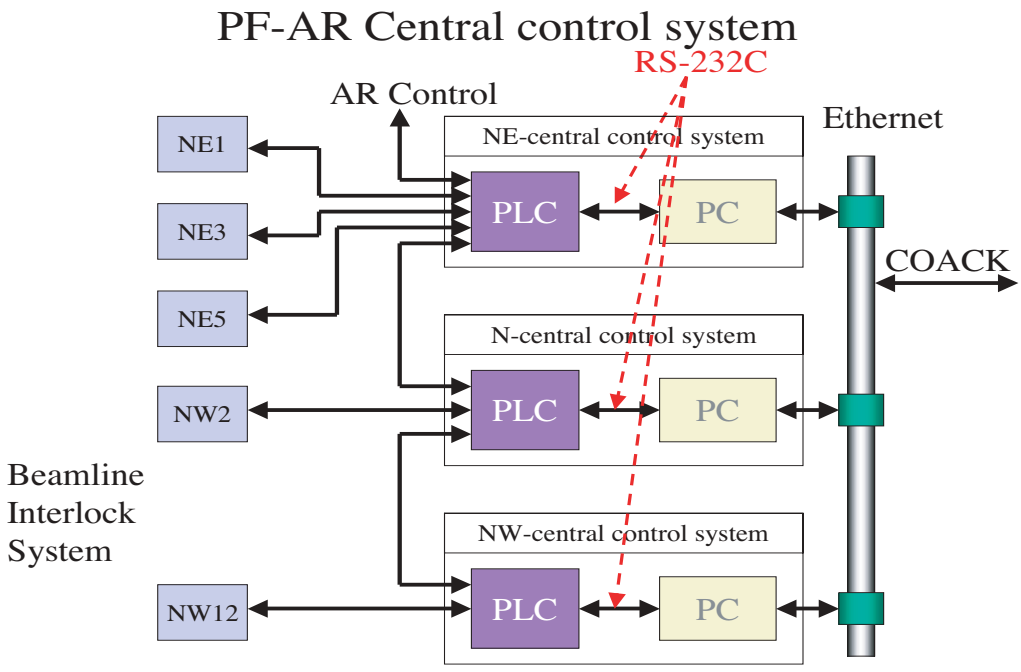

Figure 7
Schematic of a new PF-AR Central Control System.

4 Activities of the Structural Biology Research Group, Present and Future

As reported in the previous volume, the Structural Biology Group was initiated by Prof. S. Wakatsuki in May 2000. At present, the group consists of seven faculty members, four post doctoral fellows, two Ph.D. graduate students and seven supporting staff. The two main functions of the group are developing state-of-the-art facilities for modern synchrotron X-ray protein crystallographic studies and a strong in-house structural biology research program. We are pursuing them vigorously with two competitive grants from the MEXT (the Ministry of Education, Culture, Sports, Science and Technology), "Special Coordination Funds for Promoting Science and Technology" and "Protein 3000". The group covers a wide range of expertise including beam line development and operation, data acquisition and analyses systems, robotics for high-throughput structure determination, molecular biology, biochemistry, and protein X-ray crystallography. The group will play a key role in the nationwide effort of developing high-throughput protein X-ray crystallography techniques and the target oriented structural genomics (SG) project.

4-1 Upgrading of the Experimental Facilities of the Biology Laboratories

Immediately after the completion of the Structural Biology Building in March 2001, we started biological experiments focused on protein transport. Using part of the Special Coordination Funds for Promoting Science and Technology from the MEXT, we have made a substantial improvement of the experimental facilities (Fig. 1). As basic experimental instruments, we have added culture incubators, refrigerated centrifuges, a thermal cycler and an automated liquid chromatography system. More importantly, we have equipped the laboratories with more advanced biochemical instruments such as a DNA sequencer, a peptide sequencer, a fluorescence spectrophotometer, a circular dichroism spectropolarimeter, and a surface plasmon resonance sensor system (BIAcore). Thus the Structural Biology Group has now state-of-the-art facilities for comprehensive structural biology research including sample preparation and biochemical analysis.

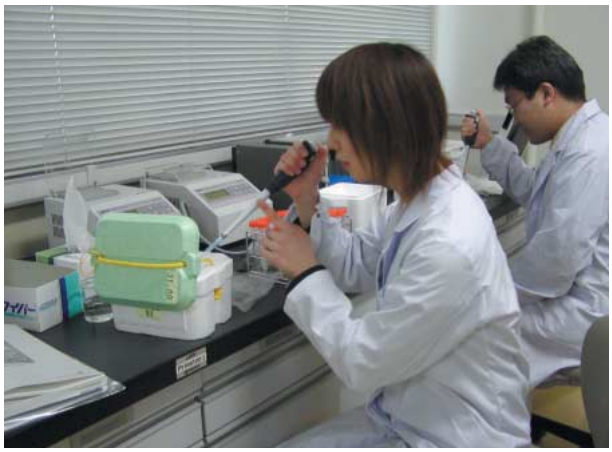

Figure 1
Biological experiments in the Structural Biology Laboratory.

4-2 Development of Automated Crystal Handling System and Unified Database

In order to facilitate high-throughput structural analysis of a large number of protein crystals, we are developing a fully automated X-ray structural analysis system. It consists of several subsystems for protein crystallization, storage, monitoring of crystal growth, harvesting and freezing crystals, mounting inside a hutch, and data acquisition.

Here, we describe the concept of the overall system. First, the storage system receives and stores trays from the crystallization system using a tray-handling robot. Status of crystallization drops is checked by the monitoring system at a pre-programmed time interval using an all-in-focus camera. A crystal that has grown large enough for X-ray analysis is sent to the next stage with the relevant information such as size and number of crystals in the drop. The crystal harvesting system (Fig. 2) then decides an appropriate size of a loop, picks one crystal up and replaces its mother liquor with a suitable cryoprotectant if necessary using a combination of an industrial robot and a purpose-built micromanipulator. The crystal is then plunged into liquid nitrogen and placed into a cassette. Inside an experimental hutch of a beamline, a mounting robot picks up a cryo-loop from the liquid nitrogen dewar and places it onto a motorized goniometer. The data acquisition system automatically aligns the crystal using a motorized XYZ stage of the goniometer and a CCD camera (or the all-in-focus camera mentioned above), and starts X-ray data collection. Integration of these steps into a self-consistent system is expected to enhance the overall throughput of structural genomics projects significantly. During the period of 2001, we have produced prototype

(a) (b)

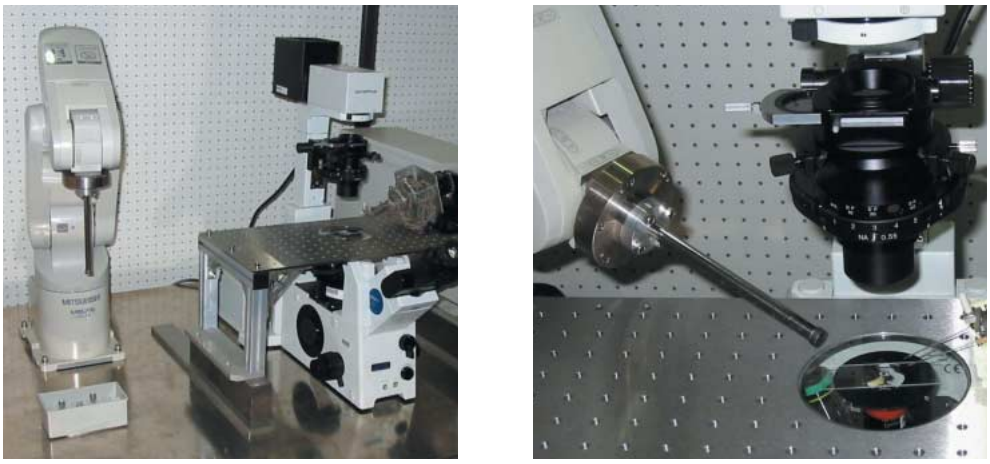

Figure 2
A prototype of an automated crystal harvesting system. (a) Overall view of the system. It consists of a handling robot, a micro manipulation arm, a microscope and a controlling PC. (b) A detailed view of the the handling robot with the micromanipulation arm on the right.

systems using a robot and micromanipulator in collaboration with Drs. T. Tanikawa and K. Ohba of Intelligent Systems Institute, National Institute of Advanced Industrial Science and Technology, Tsukuba.

It is also important to prepare an environment where a data obtained from the improved experiment equipment can be analyzed promptly and a crystal structure can be determined during a beam time. To realize this, a unified database system is being developed, which can deal with a large amount of information ranging from overexpression, purification, crystallization, X-ray diffraction data collection, data processing and structure determination. Using this system, users will be able to carry out structural studies more efficiently, because they can quickly ascertain whether the structure of the protein of interest can be determined from the present X-ray experimental data or further experiments are needed. This will also allow multiple users to monitor the progress of experiments simultaneously through the internet from several places, such as universities, research institutes, and to perform data analysis and share its results with the other collaborators.

4-3 Enhancement of the Existing Beamlines and Construction of New Beamlines

1 BL-6A

BL-6A has been in operation for almost 15 years as one of the first beamlines for protein crystallography and has contributed significantly to the progress of the field. For the last two years, BL-6A has gone through a vigorous refurbishment program aimed at higher overall performance. As the first step, a CCD-based detector system, Quantum 4R of ADSC, was installed at the end

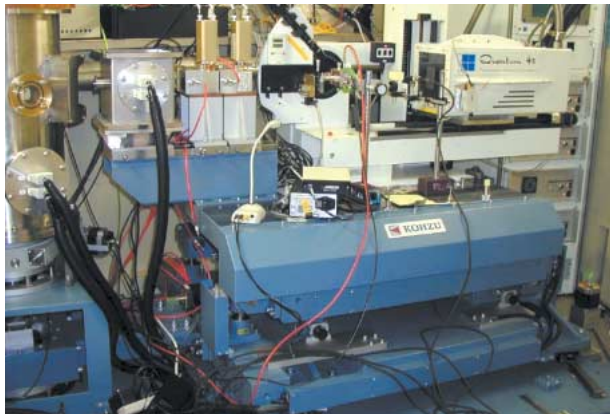

Figure 3
A new optical bench of BL-6A specifically designed for MAD experiments using a CCD detector (ADSC Quantum 4R).

of FY1999, which improved significantly the efficiency of protein crystallography experiments on the beamline. At the end of FY2000, the original optical bench was replaced by a new one specialized for MAD experiments using the CCD system (Fig. 3). At same time, new data acquisition software using the TCP/IP protocol was installed, which is expected to become the next standard of control software of the PF structural biology beamlines. With these improvements, the beamline now provides a stable, highly efficient and user-friendly data collection environment. After October 2002, it will be possible to tune the energy in the range from 0.9 Å to 1.3 Å for MAD phasing using different absorption edges: Br and Se K edges as well as L edges of typical third-raw transition elements and lanthanides.

2 AR-NW12 beamline at the PF-AR

NW12 is a new beamline designed for high-throughput protein crystallographic experiments in the PF-AR northwest experimental hall, which was completed in the end of March 2002 (Figs. 4 and 5).

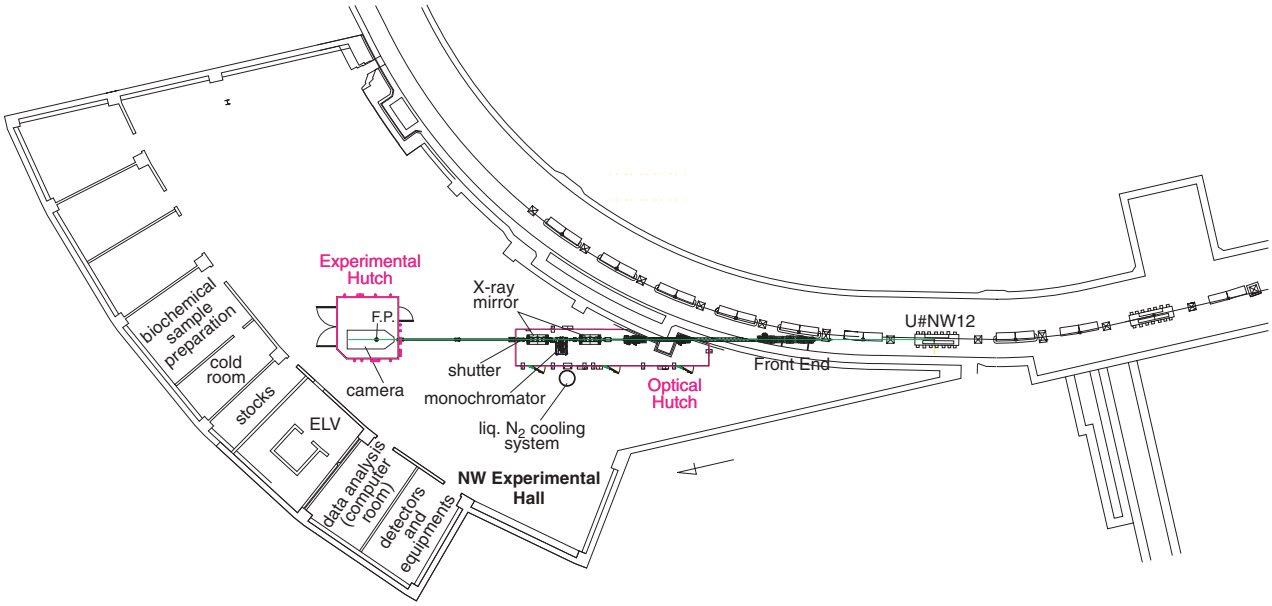

Figure 4
Schematic layout of the new beamline AR-NW12 .

Figure 5
AR-NW12 beamline under construction. The black box in the back is an optical hutch, which contains optical elements such as collimating mirror, cryogenically cooled double crystal monochromator and a focusing mirror. The brown box in front is an experimental hutch, in which an X-ray camera specialized for MAD measurements of protein crystals will be installed.

After the construction of both optical and experimental hutches in June 2002, we will start setting up optical elements in the optical hutch. The optics installation will be completed by the end of September 2002. The NW12 beamline will deliver the first beam in October 2002.

The beamline is optimized for MAD experiments, which require good energy tunability. The in-vacuum undulator of NW12 (period length: 40 mm, number of periods: 90) can cover an energy range of 7~16.8 keV using the 3rd harmonics. A flat mirror, which is installed upstream of the monochromator, is bent for vertical collimation to achieve good energy resolution (2×10^{-4} by ray tracing). The double crystal monochromator consists of flat Si(111) crystals which are cooled with liquid nitrogen in order to reduce deformation due to excessive heat loads.

NW12 is also designed as a high-flux beamline, which is expect to deliver more than 10^{12} photons/sec at the sample position, 200 × 200 μm beam size and 0.5 mrad beam divergence. A bent-cylindrical mirror after the monochromator focuses the beam into the experimental hutch (4 m × 4 m) in which an experimental table will be installed. The table has a one-circle diffractometer and a base which can hold either a standard size CCD detector or a very large area detector up to one meter active area. The sphere of confusion of the diffractometer is less than a few microns, which allow for experiments with micron size crystals.

3 New multipole wiggler beamline, BL-5, at the PF Storage Ring

We are designing a new multipole wiggler beamline for protein crystallography. The multipole wiggler is optimized at 12.7 keV for MAD experiments using Se-Met but it will cover a wide energy range from 7 keV to 16.8 keV. The beamline construction will be finished in October 2004. The specifications of the multipole wiggler are as follows:

No. of periods	20
Length of period	120 mm
Maximum magnetic field	1.4 Tesla
Total flux (/sec/0.1%bw)@12.7 keV	1×10^{15}

The beamline will consist of a collimating mirror, a double crystal monochromator and a focusing mirror. The specifications of the mirrors and the monochromator are as follows:

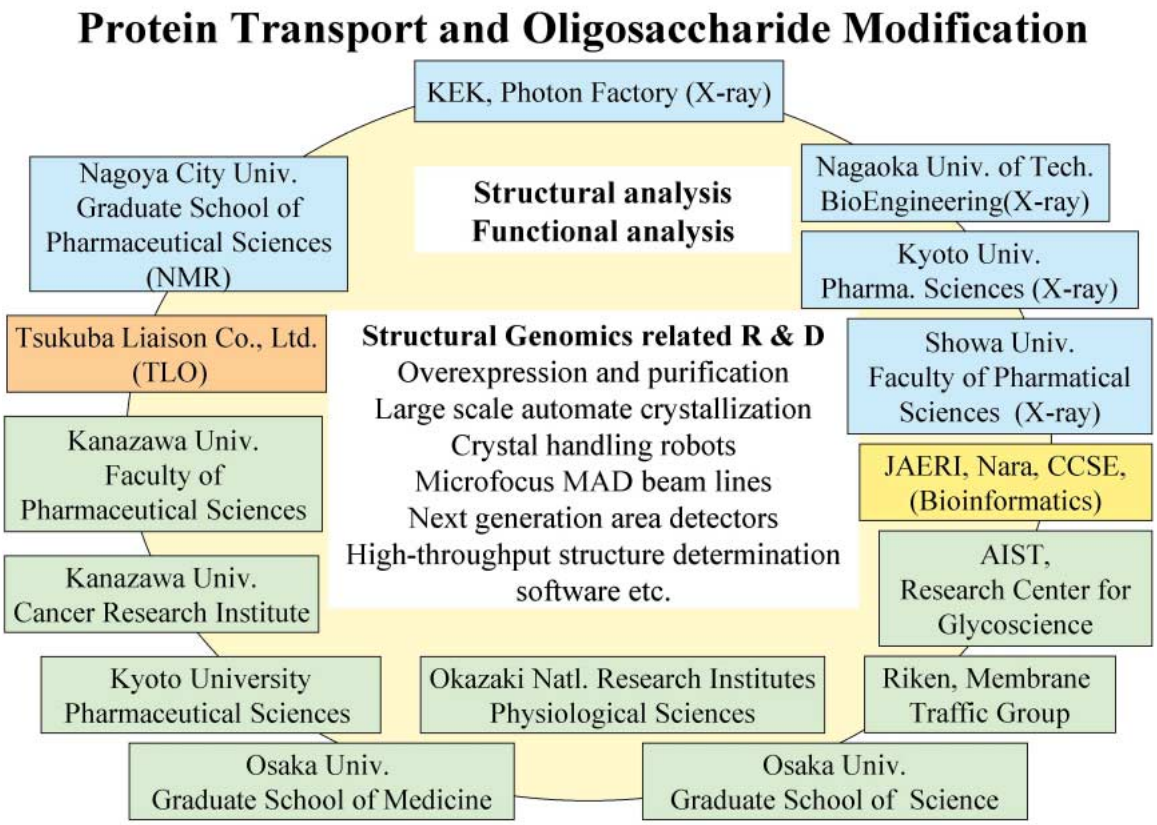

Figure 6
KEK branch of the National Project of Protein 3000.

Collimating mirror at 15.5 m
Material: rhodium-coated silicon single crystal.
Size: 1000 mm (L) × 100 mm (W) × 70 mm (H)
Radius of curvature: 8857 m
Double crystal monochromator at 20 m
Material : Si(111)
Fixed-exit type
Toroidal focusing mirror at 22 m
Material: rhodium-coated silicon single crystal.
Size: 1000 mm (L) × 100 mm (W) × 70 mm (H)
Radii of curvature: 44.71 mm, 5143 m
Focal point at 31 m
Estimated flux is >10^{11} photons/sec through 200-μm slit

4-4 Target Oriented Structural Proteomics on Post-Translational Modification and Intracellular Transport (a Project of Protein 3000)

There are many national and international post-genome projects started in the last few years. The Life Sciences Division of the MEXT is starting a five-year project of determining 3,000 protein structures or unique folds from FY2002. The structural genomics project at RIKEN will carry out the major part of the Protein 3000 project. Their primary goal is to contribute to the worldwide effort of determining all the representative structures in the structure space by determining 2,500 structures in the next five years. On the other hand structural biologists of the Japanese universities and the KEK-PF have been proposing a network of structural genomics consortia to pursue target-oriented structural genomics projects aimed at specific biological or medical targets. Each consortium consists of X-ray protein crystallography, NMR, and bioinformatics groups tightly coupled with those specialized in medical, pharmaceutical and biological sciences that share the same biological interests in their pursuit of structure-function relationships.

The Structural Biology Group of the KEK-PF organizes a consortium, as one of the eight consortia selected in Japan, to carry out a target oriented structural biology of protein modification and transport processes (Fig. 6). Protein modification and sorting are essential for all living cells. In higher organisms such as human, newly synthesized proteins need to be modified and directed to their correct targets for proper function. Error in modifying proteins and/or mis-targeting of proteins into wrong compartments cause a number of human diseases. Furthermore, infection and proliferation of viruses such as HIV and influenza require host cell's transport systems. Hence, elucidation of detailed

mechanisms of protein modification and transport is expected to lead to development of new drugs against diseases caused by viruses or mis-targeted proteins. In the long run, full understanding of these mechanisms will be extremely useful in developing key technologies to produce medically/biologically active human glycoproteins (proteins modified with short sugar chains) using lower organisms such as yeast. To pursue these lines of research, together with six universities and four institutes, the PF group has started a structural proteomics project on protein transport and post-translational modification of proteins, as one of the consortia mentioned above. Our project includes systematic structural analyses of proteins and complexes involved in the transport and oligosaccharide modification processes, as well as development of key high-throughput techniques using synchrotron radiation.

List of participating groups:

Koichi KATO,
Nagoya City University, Faculty of Pharmacology (NMR)

Hiroaki KATO,
Kyoto University, Faculty of Pharmacology (X-ray)

Takamasa NONAKA,
Nagaoka University of Technology (X-ray)

Nobutada TANAKA,
Showa University, Faculty of Pharmacology (X-ray)

Kazuhisa NAKAYAMA,
Kanazawa University, Faculty of Pharmacological Sciences

Hiroshi OHNO,
Kanazawa University, Cancer Institute

Yoshifumi JIGAMI,
AIST (National Institute of Advanced Industrial Science and Technology), Research Center for Glycoscience

Toshisuke KAWASAKI,
Kyoto University, Faculty of Pharmacology

Masayuki MURATA,
Okazaki National Research Institutes, Center for Integrative Bioscience

Akihiko NAKANO,
RIKEN Central Institute, Membrane Traffic Group

Naoyuki TANIGUCHI,
Osaka University, Medical School

Sumihiro HASE,
Osaka University, Faculaty of Science

Kei YURA,
JAERI (Japan Atomic Energy Research Institute), CCSE (Center for Promotion of Computational Science and Engineering)

Akira TASAKI,
Tsukuba Liaison Co. Ltd., Managing Director

We are also setting up a mid-size protein production facility in the PF to provide a major part of protein samples for the consortium.

As the initial step, the PF group had started systematic structural studies on the vesicle transport of glycosylated proteins from the trans-Golgi network to early lysosomes in collaboration with Dr. K. Nakayama of Kanazawa University. This collaboration has resulted in the elucidation of the recognition mechanisms of the acidic dileucine motif signal of mannose-6-phosphate receptor by the VHS domain of human GGA protein [1] and the interaction between the ear domain of γ1 adaptin of the AP-1 complex and γ-synergin and Rabaptin-5 [2] (please see the Highlights 8-3 in this issue).

Further details can be found on the web site of the group: http://pfweis.kek.jp/index_ja.html in Japanese and http://pfweis.kek.jp/index_eg.html in English.

References

[1] T. Shiba, H. Takatsu, T. Nogi, N. Matsugaki, M. Kawasaki, N. Igarashi, M. Suzuki, R. Kato, T. Earnest, K. Nakayama, and S. Wakatsuki, *Nature* **415** (2002) 937.

[2] T. Nogi, Y. Shiba, M. Kawasaki, T. Shiba, N. Matsugaki, N. Igarashi, M. Suzuki, R. Kato, H. Takatsu, K. Nakayama, S. Wakatsuki, *Nature Structural Biology* **9** (2002) 527.